

Perturbation-Assisted Sample Synthesis: A Novel Approach for Uncertainty Quantification

Yifei Liu, Rex Shen, Xiaotong Shen[✉]

Abstract—This paper introduces a novel generator called Perturbation-Assisted Sample Synthesis (PASS), designed for drawing reliable conclusions from complex data, especially when using advanced modeling techniques like deep neural networks. PASS utilizes perturbation to generate synthetic data that closely mirrors the distribution of raw data, encompassing numerical and unstructured data types such as gene expression, images, and text. By estimating the data-generating distribution and leveraging large pre-trained generative models, PASS enhances estimation accuracy, providing an estimated distribution of any statistic through Monte Carlo experiments. Building on PASS, we propose a generative inference framework called Perturbation-Assisted Inference (PAI), which offers a statistical guarantee of validity. In pivotal inference, PAI enables accurate conclusions without knowing a pivotal’s distribution as in simulations, even with limited data. In non-pivotal situations, we train PASS using an independent holdout sample, resulting in credible conclusions. To showcase PAI’s capability in tackling complex problems, we highlight its applications in three domains: image synthesis inference, sentiment word inference, and multimodal inference via stable diffusion.

Index Terms—Diffusion, High-dimensionality, Multimodality, Normalization Flows Large pre-trained Models, Uncertainty Quantification.

I. INTRODUCTION

Uncertainty quantification is crucial for scientific inquiry and drawing reliable conclusions from data, especially working with complex modeling techniques such as deep neural networks. Despite recent advancements showcasing the potential of Artificial Intelligence in facilitating data-driven discoveries, a reproducibility crisis has emerged in various fields, including biomedicine and social sciences, occasionally leading to false discoveries [17]. A key issue contributing to this crisis is the lack of methods for quantifying uncertainty in over-parametrized models, like neural networks, prioritizing predictive accuracy using many non-learnable parameters such as hyperparameters. As a result, these studies may become exaggerated and irreproducible. To address these challenges, we develop a generative inference framework designed to provide uncertainty quantification for data of any type.

This paper presents a novel Perturbation-Assisted Inference (PAI) framework that utilizes the Perturbation-Assisted Sample

Synthesis (PASS) generative model, ensuring validity as if we had conducted Monte Carlo simulations with a known data-generating distribution. PASS estimates the data-generating distribution to create synthetic data that closely mirrors the original data, encompassing numerical and unstructured data, such as images and text. Most importantly, PASS can leverage pre-trained generative models to transfer knowledge for improved accuracy in learning the data-generating distribution. Unlike other generative models, PASS focuses on inference, increasing the diversity of synthetic data, or concealing the original data for privacy protection through data perturbation, while maintaining the original sample’s ranks for personalization and data integration [2].

The PAI framework is a powerful approach to statistical inference, particularly for unstructured, multimodal, and numerical data. Utilizing synthetic data generated by PASS, PAI can simulate any statistic’s distribution and characteristics through Monte Carlo experiments, including the null distribution and the distribution conditioning an event of interest. PAI expands the scope of statistical inference to less explored areas in unstructured and multimodal data, although it directly applies to numerical data. The framework offers several key advantages compared to the classical approach, with four primary contributions:

- (1) **Inference for Unstructured and Multimodal Data.** The PAI framework broadens the scope of statistical inference from numerical to unstructured and multimodal data through synthetic data generation. Section V demonstrates the validity of PAI when PASS estimates the data-generating distribution via pre-trained generative models such as normalizing flow or diffusion models.
- (2) **Pivotal Inference.** PAI offers exact inference for any pivotal while controlling the Type-I error, which surpasses classical methods that necessitate knowledge of a test statistic’s distribution, as supported by Theorem 2.
- (3) **General Inference.** The PAI framework enables approximate inference for non-pivotal statistics while maintaining control over Type-I error rates. It achieves this by using an estimated distribution well approximating the data-generating distribution, as illustrated in Theorem 1.
- (4) **Accounting for Modeling Uncertainty.** Unlike traditional methods, PAI takes modeling uncertainty into account through Monte Carlo experiments for uncertainty assessment, which yields more valid conclusions.

The PAI framework offers improved accuracy and broader

This work was supported in part by NSF grant DMS-1952539, and NIH grants R01AG069895, R01AG065636, R01AG074858, U01AG073079. (Corresponding author: Xiaotong Shen.)

Yifei Liu is with School of Statistics, University of Minnesota, MN, 55455 USA (email: liu00980@umn.edu).

Rex Shen is with Department of Statistics, Stanford University, CA, 94305 USA (email: rshen0@stanford.edu).

Xiaotong Shen is with School of Statistics, University of Minnesota, MN, 55455 USA (email: xshen@umn.edu).

applicability compared to classical statistical inference methods. This approach yields an estimated distribution of a test statistic through an estimated data-generating distribution, enabling finite-sample inference. It contrasts with the classical approach that might require bias correction like Debiased Lasso [51]. Unlike the resampling method, PAI yields independent synthetic samples for inference while permitting data integration, sensitivity analysis, and personalization.

To demonstrate PAI’s capabilities, we address the problem of statistical inference in three challenging, previously unexplored areas, including (1) image synthesis, (2) sentiment analysis via DistilBERT [40], and (3) multimodal inference for text-to-image generation given text prompt. In these applications, PAI provides uncertainty quantification for generative models involving hyperparameter tuning, where it accounts for the statistical uncertainty of hyperparameter tuning in inference while utilizing pre-trained models to enhance the accuracy of learning the data-generating distribution. Recent studies have emphasized the importance of sample splitting in inference to prevent data snooping [4], [49]. As illustrated in these applications, PAI conducts novel hypothesis tests concerning image matching, word inference in sentiment analysis, and generated images given disparate text prompts via stable diffusion, offering uncertainty quantification for numerical and unstructured data, where neither test is analytically tractable.

This paper comprises nine sections. Section II establishes the foundation of PASS, which can estimate any statistic’s distribution via Monte Carlo experiments. Section III introduces the perturbation-assisted inference (PAI) framework based on PASS. Section IV provides a statistical guarantee of PAI’s validity. Section V develops novel tests for comparing synthetic images generated by diffusion models ([44], [19]) and other deep generative models such as GLOW [24] and DCGAN [35], for assessing the feature importance of positive, negative, and neutral words in sentiment analysis via DistilBERT, and for multimodal inference from texts to images. Section VI presents numerical experiments. The Appendix contains some technical details. The Supplementary Material contains additional results of learning theory for normalizing flows.

II. PERTURBATION-ASSISTED SAMPLE SYNTHESIS

Given a d -dimensional random sample $\mathbf{Z} = (\mathbf{Z}_i)_{i=1}^n$ from a cumulative distribution function (CDF) $F_{\mathbf{Z}}(\cdot) = F_{\mathbf{Z}}(\cdot; \boldsymbol{\theta})$, or data-generating distribution, $\mathbf{Z}_i \sim F_{\mathbf{Z}}; i = 1, \dots, n$, we estimate a statistic $H(\mathbf{Z})$ ’s distribution, where $\boldsymbol{\theta}$ is a vector of unknown parameters and H is a vector of known functions that may be analytically intractable. Here, \mathbf{Z} could be an independently and identically distributed sample or its continuous latent vector representation obtained through, for example, a latent normalizing flow ([34], [52]) and VAE [25] for images and a numerical embedding such as BERT-style transformer for texts. Subsequently, we assume that $F_{\mathbf{Z}}$ is absolutely continuous and use the continuous latent vectors of unstructured data or a continuous surrogate of non-continuous data [2] for a downstream task.

A. Sample Synthesis

Generation via Transport. To generate a random sample $\mathbf{Z}' = (\mathbf{Z}'_i)_{i=1}^n$ from a cumulative distribution $F_{\mathbf{Z}}$, we construct a transport G mapping a base distribution of \mathbf{U} to that of \mathbf{Z} , preferably simple, like the Uniform or Gaussian, where $\mathbf{U} = (\mathbf{U}_i)_{i=1}^n$ is a sample from the base distribution $F_{\mathbf{U}}$. In the univariate case, we generate $\mathbf{Z}'_i = G(\mathbf{U}_i)$ by choosing $G = F_{\mathbf{Z}}^{-1}$ with \mathbf{U}_i sampled from the Uniform distribution $U[0, 1]; i = 1, \dots, n$. However, this generative method is no longer valid in the multivariate case as the multivariate analogy of $F_{\mathbf{Z}}^{-1}$ does not exist. In such a situation, the reconstruction of G mapping \mathcal{R}^d to \mathcal{R}^d is challenging.

Linkage between Generated and Original Data. Sample \mathbf{Z}' generated from the base distribution of \mathbf{U} may not accurately represent \mathbf{Z} if they are unrelated to \mathbf{Z} . When $d = 1$, \mathbf{Z}' retains the ranks of \mathbf{Z} if \mathbf{U} retains the ranks of \mathbf{Z} , by the non-decreasing property of $G = F_{\mathbf{Z}}$. As argued in [2], \mathbf{Z}' connects to the original sample \mathbf{Z} by rank preservation. This aspect is crucial for personalized inference, outlier detection, and data integration. To generalize this concept of rank preservation to the multivariate situation, we consider a transport T mapping from $F_{\mathbf{Z}}$ to $F_{\mathbf{U}}$, which is not necessarily invertible. However, the invertibility ensures a round-trip transformation between $F_{\mathbf{Z}}$ and $F_{\mathbf{U}}$ is uniquely determined. We then align the multivariate ranks of $(\mathbf{U}_i)_{i=1}^n$ with those of $(T(\mathbf{Z}_i))_{i=1}^n$, which preserves the ranks of $(\mathbf{Z}_i)_{i=1}^n$ using its representation $(T(\mathbf{Z}_i))_{i=1}^n$ in the space of the base variables \mathbf{U} . The reader refers to Appendix B for further details on multivariate ranks. In other words, this alignment preserves the ranks of $(\mathbf{Z}_i)_{i=1}^n$ by $(\mathbf{U}_i)_{i=1}^n$ when T is invertible and recovers the univariate case. In practice, we may reconstruct G with $T = G^{-1}$ as in the case of normalizing flow or treat a non-invertible T separately as in a diffusion model; see subsequent paragraphs for examples.

Perturbation for Diversity and Protection. Recent research in denoising diffusion models ([38], [44], [10]) has demonstrated that adding Gaussian noise in the forward diffusion process and subsequent denoising to estimate the initial distribution $F_{\mathbf{Z}}$ in the reverse process can effectively improve the diversity of generated samples. Moreover, adding noise in a certain form of data perturbation [41] can allow \mathbf{Z}' to satisfy the differential privacy standard [2] for privacy protection.

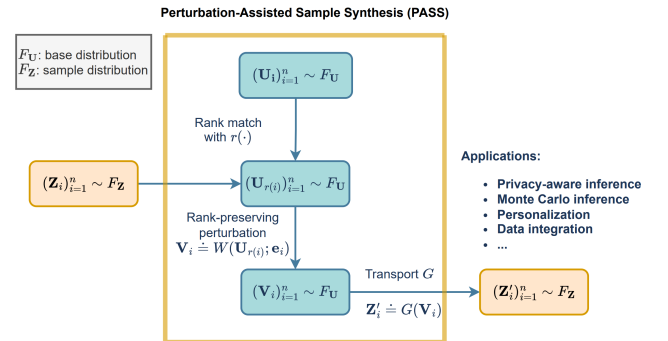


Fig. 1. Flow chart for PASS using rank-preserving perturbation in the latent representation space. The transport G is applied to recover the data in the original sample space.

This discussion leads to the generation scheme of PASS, which comprises three components, transport estimation, rank preservation, and data perturbation:

- (1) Sample $\mathbf{U} = (\mathbf{U}_i)_{i=1}^n$ from the base distribution F_U ;
- (2) Compute the permutation map $r(\cdot)$ on $\{1, \dots, n\}$ to align the multivariate ranks of $(\mathbf{U}_{r(i)})_{i=1}^n$ with those of $(T(\mathbf{Z}_i))_{i=1}^n$, where T is a transport map from F_Z to F_U . See Appendix B for more information about $r(\cdot)$.
- (3) Generate $\mathbf{Z}' = (\mathbf{Z}'_i)_{i=1}^n$ by adding noise $(\mathbf{e}_i)_{i=1}^n \sim F_e$:

$$\mathbf{Z}'_i = G(\mathbf{V}_i), \quad \mathbf{V}_i = W(\mathbf{U}_{r(i)}; \mathbf{e}_i); i = 1, \dots, n, \quad (1)$$

where W is a known perturbation function that injects noise to \mathbf{U} while preserving the base distribution, that is, $(\mathbf{V}_i)_{i=1}^n$ will still be random sample from $F_V = F_U$, and G is a transport map that pushes F_V to F_Z . An illustration is provided in Fig 1.

Notable is that the equation (1) can be applied to embeddings of original data for dimension reduction, as demonstrated in studies such as [38], [44], [10]. In (1), G and T represent generation and rank preservation, respectively. For simplicity, we estimate G by assuming its inevitability. However, in certain cases, it is advantageous not to impose the invertibility on G while estimating T separately, as in diffusion models. As for perturbation, we can select W to preserve the multivariate ranks of $(\mathbf{U}_{r(i)})_{i=1}^n$ by \mathbf{V}_i , even after adding noise $(\mathbf{e}_i)_{i=1}^n$ (see Theorem 3). For example, Appendix C presents an additive form of W . Regarding the noise distribution F_e , we typically parametrize it as $\mathbf{e} = \tau \epsilon$, with $\tau > 0$ denoting the perturbation size and $\epsilon \sim F_e$ representing a standardized noise distribution. When privacy is not a concern, we can conveniently set $\tau = 0$ and select W as the identity map. Additionally, when personalization and data integration are not the primary focus, as in Section V, we can choose $r(i) = i$; $i = 1, \dots, n$.

Separation of (G, T) from a Downstream Task. Ideally, we can repurpose the original sample \mathbf{Z} to estimate the transports G and T while executing a downstream task. However, this approach is debatable regarding the validity of the downstream analysis [8]. Whereas it offers valid inference for a pivotal statistic $H(\mathbf{Z})$, as demonstrated in Theorem 2, it may yield overly optimistic conclusions in post-selection inference [8]. To circumvent this problem, we recommend using an independent holdout sample, usually available from other studies on the same population. For example, training examples for similar images could serve as holdout data to learn the data-generating distribution for inference, as illustrated in Section VI. By separating downstream analysis from estimating G and T , we guarantee the validity of an inference even with a finite sample size; see Theorem 2. If holdout data is unavailable, a possible alternative is sample splitting, with one subsample acting as a holdout sample. This method can yield valid conclusions but may compromise statistical power [50].

B. Data-Generating Distribution

Given a holdout sample $\mathbb{S}_h = (\mathbf{Z}_i)_{i=1}^{n_h}$, our objective is to construct \tilde{F}_Z , or equivalently \tilde{G} , in order to estimate the data-generating distribution $F_Z = F_V \circ G^{-1}$. Building on this

foundation, PASS generates $\mathbf{Z}' = (\mathbf{Z}'_i)_{i=1}^n$ following \tilde{F}_Z , as detailed in Lemma 1. Subsequently, we propose employing generative models to reconstruct \tilde{F}_Z , either *explicitly* by approximating G with an invertible \tilde{G} , as in $\tilde{F}_Z = F_V \circ \tilde{G}^{-1}$, or *implicitly* through sampling, which we discuss further below. Consequently, large pre-trained generative models can enhance the estimation accuracy of the data-generating distribution.

Explicit Estimation. We suggest estimating G by maximizing a likelihood function $L(G; \mathbb{S}_h)$, which is parameterized through the distribution of \mathbf{V} . Specifically, we obtain an estimated transport \tilde{G} by

$$\tilde{G} = \arg \min_{G \in \mathcal{F}} (L(G; \mathbb{S}_h) + \lambda P(G)), \quad (2)$$

where \mathcal{F} is a predefined function class, such as normalization flows, $P(G)$ is a nonnegative penalty function, and $\lambda \geq 0$ is a regularization parameter. In (2), its constrained version can serve the same purpose, as described by [42]. Furthermore, due to the nature of \tilde{G} , we can explicitly obtain the analytical form of \tilde{F}_Z and the corresponding density. Refer to subsequent details for illustration.

Normalizing Flows. [24], [11], [12] uses a sequence of composited diffeomorphism to approximate $G = T_\theta = T_{\theta_K} \circ \dots \circ T_{\theta_1}$ in (1), where each T_{θ_k} is a simple diffeomorphism parametrized by θ_k , for instance, a deep net, and $\theta = (\theta_1, \dots, \theta_K)$. Note, the probability densities of \mathbf{Z} and \mathbf{V} $p_Z(\mathbf{z}; \theta) = p_V(G^{-1}(\mathbf{z})) |\det J_{G^{-1}}(\mathbf{z})|$ and p_V , where $J_{G^{-1}}$ is the Jacobian of G^{-1} and \det represents determinant. Then, $L(G; \mathbb{S}_h)$ in (2) can be written as $L(G; \mathbb{S}_h) = \sum_{i=1}^{n_h} \log p_Z(\mathbf{Z}^{(i)}; \theta)$ where $\log p_Z(\mathbf{z}; \theta) = \log p_V(\mathbf{z}^{(0)}) - \sum_{k=1}^K \log |\det J_{T_{\theta_k}}(\mathbf{z}^{(k-1)})|$, where $\mathbf{z}^{(0)} = \mathbf{v} = G^{-1}(\mathbf{z})$, $\mathbf{z}^{(k)} = T_{\theta_k}(\mathbf{z}^{(k-1)})$, and $\mathbf{z}^{(K)} = \mathbf{z}$. Given simple structures of T_{θ_k} , both G^{-1} and $|\det J_{T_{\theta_k}}(\mathbf{z}^{(k-1)})|$ can be easily evaluated, for example, the affine coupling flow [12] and the autoregressive flow [15].

Implicit Estimation. In certain situations, it is convenient to estimate F_Z implicitly, via sampling. When the dimension of G is low, we may reconstruct the target distribution \tilde{F}_Z using a smoothed empirical CDF. For example, [2], [41] use the chain rule to construct such a \tilde{G} coordinate-wise. In high-dimensional situations, especially for unstructured data, we adopt state-of-the-art generative models such as diffusion models ([44], [19]) to reconstruct \tilde{G} .

A **diffusion model** involves a forward process and a reverse process. Given a random vector \mathbf{Z}_0 from a d -dimensional data-generating distribution F_Z , the forward diffusion process adds white noise to the sample gradually in T steps, producing noisy $\mathbf{Z}_0: \mathbf{Z}_1, \dots, \mathbf{Z}_T: \mathbf{Z}_t = \sqrt{1 - \beta_t} \cdot \mathbf{Z}_{t-1} + \sqrt{\beta_t} \cdot \epsilon_t$, with $\epsilon_t \sim N(\mathbf{0}_d, \mathbf{I}_d)$. Here, a variance schedule $\beta_t \in (0, 1)$ controls the amount of noise at step t for \mathbf{Z}_T to approximate white noise $N(\mathbf{0}_d, \mathbf{I}_d)$. On the other hand, during the reverse diffusion process, we start with $\mathbf{Z}_T \sim N(\mathbf{0}_d, \mathbf{I}_d)$ and progressively subtract noises to generate data $\mathbf{Z}_T, \mathbf{Z}_{T-1}, \dots, \mathbf{Z}_0$ such that the generated sample $\mathbf{Z}' \equiv \mathbf{Z}_0 \sim F_Z$ approximately: $\mathbf{Z}_{t-1} = \mu_\theta(\mathbf{Z}_t, t) + \sqrt{\beta_t} \epsilon_t$, $\epsilon_t \sim N(\mathbf{0}_d, \mathbf{I}_d)$, where $\mu_\theta(\mathbf{Z}_t, t) = \frac{1}{\sqrt{1 - \beta_t}} (\mathbf{Z}_t - \frac{\beta_t}{\sqrt{1 - \prod_{i=1}^t (1 - \beta_i)}} \cdot \epsilon_\theta(\mathbf{Z}_t, t))$ [19] is a denoising function, and $\epsilon_\theta(\mathbf{Z}_t, t)$ is a neural network, such as U-net [39], parameterized by θ , predicting the noise

in \mathbf{Z}_t . The loss based on a training sample $\mathbb{S}_h = (\mathbf{Z}_i)_{i=1}^{n_h}$, derived from evidence lower bound of the likelihood, is: $L(\boldsymbol{\theta}) = \sum_{t=1}^T \mathbb{E} [\|\epsilon_t - \epsilon_{\boldsymbol{\theta}}(\mathbf{Z}_t, t)\|_2^2]$, where the expectation is taken regarding $(\epsilon_t)_{t=1}^T$ and $\|\cdot\|$ is the L_2 -norm. Given a trained neural network, we sample $\mathbf{Z}_T = \mathbf{V}$ from the white noise and iteratively apply the denoising function $\mu_{\boldsymbol{\theta}}(\cdot, t)$ T steps to obtain the final synthesized sample $\mathbf{Z}' = \tilde{G}(\mathbf{Z}_T)$, that is, $\tilde{G} = \mu_{\boldsymbol{\theta}}(\cdot, 1) \circ \dots \circ \mu_{\boldsymbol{\theta}}(\cdot, T)$.

Distribution Estimation of a Statistic $H(\mathbf{Z})$ by PASS.

Given an estimate \tilde{G} , we can obtain an estimated distribution $\tilde{F}_{\mathbf{Z}} = F_{\mathbf{V}} \circ \tilde{G}^{-1}$ when \tilde{G} is invertible. Notably, PASS can generate synthetic samples using $\mathbf{Z}' = \tilde{G}(\mathbf{V}) \sim \tilde{F}_{\mathbf{Z}}$ derived from (1). Based on this, we propose a Monte Carlo method for estimating the CDF $F_{H(\mathbf{Z})}$ of any statistic $H(\mathbf{Z})$. Specifically, we generate D independent synthetic samples $(\mathbf{Z}'^{(d)})_{d=1}^D$ using (1), and construct the PASS estimate as an empirical CDF: $\tilde{F}_{H(\mathbf{Z}')}(\mathbf{x}) = D^{-1} \sum_{d=1}^D I(H(\mathbf{Z}'^{(d)}) \leq \mathbf{x})$ for estimating F_H , where each $\mathbf{Z}'^{(d)}$ is from $\tilde{F}_{\mathbf{Z}}$ by PASS. Refer to Section IV for statistical guarantee and justification of this approach.

C. Sampling Properties of PASS

Lemma 1 presents the sampling properties of \mathbf{Z}' generated by PASS.

Lemma 1. (Sampling properties of PASS) Given $\mathbf{Z}' = (\mathbf{Z}'_i)_{i=1}^n$ generated from (1) using \tilde{G} , assume that $\tilde{F}_{\mathbf{Z}}$ is independent of $\mathbf{Z} = (\mathbf{Z}_i)_{i=1}^n$. Then,

- 1) (Within-sample) $\mathbf{Z}' = (\mathbf{Z}'_i)_{i=1}^n$ is an independent and identically distributed (iid) sample of size n according to $\tilde{F}_{\mathbf{Z}}$ when \mathbf{Z} is independent and identically distributed.
- 2) (Independence) $H(\mathbf{Z}')$ is independent of \mathbf{Z} for any permutation-invariant H in that $H(\mathbf{Z}) = H(\mathbf{Z}_{\pi})$ with $\mathbf{Z}_{\pi} = (\mathbf{Z}_{\pi(i)})_{i=1}^n$, where π represents any permutation map on $\{1, \dots, n\}$.

Lemma 1 highlights the two advantages of a generated PASS sample \mathbf{Z}' . First, its iid property is unique and not shared by any resampling approach. Second, the conditional distribution of the PASS statistic $H(\mathbf{Z}')$ given \mathbf{Z} is the same as its unconditional distribution, a property not shared by existing resampling methods. This aspect is somewhat surprising because the permutation invariance of a test statistic H allows for rank preservation of \mathbf{Z}' without imposing dependence between \mathbf{Z}' and \mathbf{Z} . Note that a common test statistic H is invariant concerning the permutation of the sample order for an iid sample [21]. These two aspects ensure that the PASS sample $H(\mathbf{Z}')$ accurately represents $H(\mathbf{Z})$, leading to a reliable estimate of the distribution of $H(\mathbf{Z})$.

III. PERTURBATION-ASSISTED INFERENCE

For inference, data scientists often use a statistic $H(\mathbf{Z})$ for hypothesis testing or a confidence interval concerning $\boldsymbol{\theta}$ or its functions. Based on the PASS framework described in Section II, we estimate the distribution of $H(\mathbf{Z})$, which permits a valid inference through Monte Carlo simulation. We introduce a generative inference framework called Perturbation-Assisted Inference (PAI). PAI involves two independent samples: an

inference sample $\mathbb{S} = (\mathbf{Z}_i)_{i=1}^n$ via $H(\mathbf{Z})$ and a holdout sample $\mathbb{S}_h = (\mathbf{Z}_i)_{i=1}^{n_h}$ for estimating the generating distribution via PASS. However, if $H(\mathbf{Z})$ is pivotal, then holdout and inference samples can be the same, as suggested by Theorem 2.

To perform a hypothesis test or construct a confidence interval, we proceed as follows:

- (1) **Estimation of Null Distribution of $H(\mathbf{Z})$.** Under the null hypothesis H_0 , we use the holdout sample \mathbb{S}_h for the data-generating distribution of PASS in (1) to estimate the null distribution of a test statistic $H(\mathbf{Z})$, which avoids sample reuse. Specifically, we generate D independent copies of synthetic samples $\mathbf{Z}'^{(d)}$; $d = 1, \dots, D$ via (1), where $\tilde{F}_{\mathbf{Z}}(\cdot) = F_{\mathbf{Z}}(\cdot; \tilde{\boldsymbol{\theta}}^0)$ with $\tilde{\boldsymbol{\theta}}^0$ being an estimate of $\boldsymbol{\theta}$ under H_0 . Then, we compute the empirical distribution $\tilde{F}_{H(\mathbf{Z}')}(\mathbf{x}) = D^{-1} \sum_{d=1}^D I(H(\mathbf{Z}'^{(d)}) \leq \mathbf{x})$ for any real \mathbf{x} as the PASS estimate of F_H given D independent copies of synthetic samples $\{\mathbf{Z}'^{(d)}\}_{d=1}^D$ via (1), where each sample $\mathbf{Z}'^{(d)}$ is from $\tilde{F}_{\mathbf{Z}}$ by PASS.
- (2) **Inference.** We use the empirical null distribution $F_{H(\mathbf{Z}')}$ to compute the rejection probability based on a trained machine learner evaluated on an inference sample \mathbb{S}_i to draw an inference. Moreover, we can convert a test into a confidence set.

Connection with Other Generative Models. PASS is compatible with various generative models for estimating the transport G in (1), which can utilize large pre-trained models to enhance the accuracy of distribution estimation. Unlike other generators, PASS maintains the ranks of an inference sample and incorporates noise to diversify or safeguard the original data.

Connection with Resampling. The resampling approach tailors for low-dimensional numerical data [13], where $F_{\mathbf{Z}}$ can be accurately estimated based on \mathbf{Z} . However, these methods struggle with high-dimensional data due to the curse of dimensionality. Additionally, the resampled data is only conditionally independent, even when \mathbf{Z} is independent. For example, in the parametric bootstrap, conditioning on $\mathbf{Z} \sim N(\boldsymbol{\mu}, \mathbf{I})$, a sample $\mathbf{Z}^B \sim N(\hat{\boldsymbol{\mu}}, \mathbf{I})$ assuming known identity covariance matrix \mathbf{I} and $\hat{\boldsymbol{\mu}}$ is the estimated mean vector from \mathbf{Z} . However, for its unconditional distribution, $\mathbb{E} \mathbf{Z}^B = \mathbb{E} \hat{\boldsymbol{\mu}}$ and $\text{Var} \mathbf{Z}^B = \text{Var} \hat{\boldsymbol{\mu}} + \mathbf{I}$. This approach can lead to overly optimistic conclusions in post-selection inference as $\hat{\boldsymbol{\mu}}$ depends on a selected model ([14], [29], [50]).

In contrast, PASS produces an independent sample when a holdout sample is independent of \mathbf{Z} , as discussed in Lemma 1, which enables valid inference. Moreover, a PASS sample preserves the ranks of an inference sample, facilitating personalization and data integration. Crucially, PASS can generate numerical, unstructured, and multimodal data, such as image-text pairs, allowing PAI to transcend the traditional inference framework and tackle complex problems involving unstructured and multimodal data inference.

IV. STATISTICAL GUARANTEE AND JUSTIFICATION

Given PASS samples $\mathbf{Z}'^{(d)}$ from $\tilde{F}_{\mathbf{Z}}$ estimated on an independent holdout sample, we provide a guarantee of validity of PAI by investigating PASS's estimation error of

$\tilde{F}_H(\mathbf{Z}')$, as measured by the Kolmogorov-Smirnov Distance: $KS(\tilde{F}_H(\mathbf{Z}'), F_H) = \sup_{\mathbf{x}} |\tilde{F}_H(\mathbf{Z}')(\mathbf{x}) - F_H(\mathbf{x})|$. Next, we perform the error analysis for non-pivotal inference and pivotal inference.

A. General Inference with Holdout

Theorem 1. (Validity of PAI) Assume that the estimated data-generating distribution by PASS on a holdout sample \mathbb{S}_h of size n_h is independent of an inference sample \mathbb{S} . Moreover, H is a permutation-invariant statistic calculated on \mathbb{S} . Then, the reconstruction error of $\tilde{F}_H(\mathbf{Z}')$ with the MC size D by PASS satisfies: for any small $\delta > 0$, with probability at least $(1 - \delta)$,

$$KS(\tilde{F}_H(\mathbf{Z}'), F_H) \leq \sqrt{\frac{\log(4/\delta)}{2D}} + |\mathbb{S}| \cdot TV(\tilde{F}_Z, F_Z), \quad (3)$$

where $TV(\tilde{F}_Z, F_Z)$ is the total variation distance between the distributions of \tilde{F}_Z and F_Z . Hence, PAI yields a valid test on \mathbb{S} provided that $|\mathbb{S}| \cdot TV(\tilde{F}_Z, F_Z) \rightarrow 0$ as $n_h \rightarrow \infty$ and $D \rightarrow \infty$.

Remark 1. Note that $|\mathbb{S}| \cdot TV(\tilde{F}_Z, F_Z) \rightarrow 0$ requires that the holdout size $n_h = |\mathbb{S}_h|$ should be larger than the inference size $n = |\mathbb{S}|$ as $TV(\tilde{F}_Z, F_Z) \rightarrow 0$ at a rate slower than n_h^{-1} .

Remark 2. For a diffusion model defined by a d -dimensional Brownian motion, Theorem 5.1 of [33] establishes the error bound between \tilde{F}_Z and F_Z : under regularity conditions:

$$E[TV(\tilde{F}_Z, F_Z)] = O(n_h^{-r/(2r+d)} (\log n_h)^{\frac{5d+8r}{2d}}),$$

where the data-generating distribution F_Z belongs to the Besov ball $B_{p,q}^r([-1, 1]^d, C)$ with radius $C > 0$ and the L_p -modulus of smoothness $r > d(1/p - 1/2)_+$, as measured by the L_q -norm ($p, q > 0$).

Remark 3. For normalizing flows, Proposition ?? in the Supplement Material provides an error bound for $TV(\tilde{F}_Z, F_Z)$ expressed in terms of the estimation and approximation errors of a flow, which implies that $TV(\tilde{F}_Z, F_Z) \rightarrow 0$ as $n_h \rightarrow +\infty$ when the approximation error tends to zero, which we expect as a flow serves as an universal approximator for complex distributions [26].

Theorem 1 suggests that the estimation error of the PASS estimate, $\tilde{F}_H(\mathbf{Z}')$, is governed by two factors: the Monte Carlo (MC) error, $\sqrt{\frac{\log(4/\delta)}{2D}}$, and the estimation error of the data-generating distribution, $TV(\tilde{F}_Z, F_Z)$. The MC error diminishes to 0 as the MC size, D , increases, while the latter depends on the estimation method of G in (1) applied to a holdout sample, \mathbb{S}_h , which in general goes to 0 as $n_h \rightarrow +\infty$. Moreover, PASS can utilize large pre-trained models to boost learning accuracy via knowledge transfer, which we may regard as an increase in n_h .

B. Pivotal Inference without Holdout

This subsection generalizes the previous result to a pivotal $H(\mathbf{Z}) = T(\tilde{\theta}, \theta)$ for parameter θ , where T is a transformation and $\tilde{\theta}$ is an estimate of θ based on \mathbf{Z} . In this situation, PAI does not require a holdout sample, $F_{\mathbf{Z}}(\cdot) = F_{\mathbf{Z}}(\cdot; \theta)$ is parametrized by θ , and $\tilde{F}_{\mathbf{Z}}(\cdot) = F_{\mathbf{Z}}(\cdot; \tilde{\theta}) = F_{\mathbf{V}} \circ G^{-1}(\cdot; \tilde{\theta})$,

Algorithm 1: PAI: Image Synthesis Inference

Input : Test image embeddings \mathbb{S}_{test} ; Generated embeddings \mathbb{S}_{fake} from a candidate generator \mathcal{G} ; PASS generator \mathcal{G}_h ; MC size D .
Output : A P-value indicating whether \mathcal{G} has similar performance compared to \mathcal{G}_h by testing (4).

```
// Calculate the test statistic
1 Compute  $T = \text{FID}(\hat{P}_{\text{test}}, \hat{P}_{\text{fake}})$  where  $\hat{P}_{\text{test}}$  and  $\hat{P}_{\text{fake}}$ 
   are empirical distributions of  $\mathbb{S}_{\text{test}}$  and  $\mathbb{S}_{\text{fake}}$ .
// Estimate the distribution of  $T$  under  $H_0$ 
2 for  $d = 1, \dots, D$  do
3   Generate  $\mathbb{S}^{(d)}$  of size  $|\mathbb{S}_{\text{fake}}|$  using  $\mathcal{G}_h$ ;
4   Compute  $T^{(d)} = \text{FID}(\hat{P}_{\text{test}}, \hat{P}^{(d)})$ , where  $\hat{P}^{(d)}$  is
   the empirical distributions of  $\mathbb{S}^{(d)}$ .
5 end
6 Compute  $F_D$ , the empirical CDF of  $(T^{(d)})_{d=1}^D$ .
// Empirical two-sided P-value
7 return P-value =  $2 \min(F_D(T), 1 - F_D(T))$ .
```

where $\tilde{\theta}$ can be any estimator of θ due to the pivotal property and (2) is no longer required. Moreover, given PASS samples $\{\mathbf{Z}'^{(d)}\}_{d=1}^D$ from \tilde{F}_Z using PASS, the PAI pivotal is $H(\mathbf{Z}'^{(d)}) = T(\tilde{\theta}^{(d)}, \tilde{\theta})$, where $\tilde{\theta}^{(d)}$ is an estimate of θ on $\mathbf{Z}'^{(d)}$; $d = 1, \dots, D$.

Theorem 2. (Validity of PAI for Pivotal Inference) The conclusion of Theorem 1 holds with $TV(\tilde{F}_Z, F_Z) = 0$ provided that $H(\mathbf{Z})$ is pivotal for θ . Hence, PAI yields a valid test on \mathbb{S} provided that $D \rightarrow \infty$.

Theorem 2 establishes that the PASS estimate $\tilde{F}_H(\mathbf{Z}')$ can exactly recover F_H without any estimation error of the data-generating distribution, provided that $H(\mathbf{Z})$ is pivotal, even though the estimation error occurs when estimating F_Z . This result improves the previous findings in [41] and justifies using an inference sample \mathbb{S} alone to estimate F_Z for making pivotal inferences.

V. APPLICATIONS

A. Image Synthesis

In image synthesis, deep generative models have been popular due to the quality of generated synthetic images from original images. Recently, researchers have demonstrated that cascaded diffusion models [20] can generate high resolution with high-fidelity images surpassing BigGan-deep [3] and VQ-VAE2 [36] on the Fréchet inception distance (FID). However, such a comparison lacks uncertainty quantification. Subsequently, we fill the gap to draw a formal inference with the uncertainty quantification for comparing two distributions.

Given two multivariate Gaussian distributions $P_0 = N(\mu_0, \Sigma_0)$ and $P = N(\mu, \Sigma)$, the FID score is defined as $\text{FID}(P_0, P) = \|\mu_0 - \mu\|_2^2 + \text{tr}(\Sigma_0 + \Sigma - 2(\Sigma\Sigma_0)^{\frac{1}{2}})$, where $\|\cdot\|_2$ is the L_2 -norm, and tr denotes the trace of a matrix. For measuring the quality of generated images, we usually calculate FID on the feature maps extracted via Inception-V3 model [46], a pre-trained vision model that has a great capacity

for extracting visual signals. In our case, P_0 and P would be the original and generated distributions of those feature maps. Here, we test

$$H_0 : \text{FID}(P_0, P) = 0, \quad H_a : \text{FID}(P_0, P) > 0. \quad (4)$$

Then, we construct a test statistic as follows: $T = \text{FID}(\hat{P}_0, \hat{P})$, the empirical FID score between the empirical distribution of test images \hat{P}_0 and that of synthesized test images \hat{P} using a trained model, on feature maps from the Inception-V3 model.

To train PASS for PAI inference, we create two independent sets of images denoted by $\mathbb{S}_h = (\mathbf{Z}_i)_{i=1}^{n_h}$ and $\mathbb{S} = (\mathbf{Z}_i)_{i=n_h+1}^{n_h+n}$ for holdout and inference, where \mathbf{Z}_i represents the i -th image. For image generation, we further split the inference sample \mathbb{S} into training and test sets for training and evaluating a generator, which is a common practice. Then, we proceed in three steps. First, we train a PASS generator on a holdout sample \mathbb{S}_h to generate the null distribution under the null that there is no difference between the PASS and the candidate generators under H_0 . Second, we train a candidate generator on the training set, with which we evaluate its performance using the test statistic $T = \text{FID}(\hat{P}_0, \hat{P})$ on the test set, where \hat{P}_0 and \hat{P} are the estimated distributions from the baseline and the candidate generator. Third, we generate D independent copies of synthetic images $(\mathbf{Z}_i^{(d)})_{i=1}^n$ from the null distribution using PASS; $d = 1, \dots, D$. Then, we compute the corresponding test statistics $(T^{(d)})_{d=1}^D$ to obtain the empirical null distribution of T on \mathbb{S} , where $T^{(d)} = \text{FID}(\hat{P}_0, \hat{P}^{(d)})$ evaluated on \mathbb{S} , and $\hat{P}^{(d)}$ is obtained on $(\mathbf{Z}_i^{(d)})_{i=1}^n$. Finally, we compute a two-sided¹ P-value using $(T^{(d)})_{d=1}^D$ and T based on \mathbb{S} ; c.f., Algorithm 1 for details.

B. Sentiment Word Inference

Given the unstructured nature of data and the complexity of modeling techniques such as transformer-based models, inferring important words for a learning task can be challenging. In this section, we perform a significance test for the feature relevance of a collection of positive, negative, and neutral words for sentiment analysis of text reviews labeled as positive or negative.

Let \mathcal{W}_M be the words of interest. Consider the null hypothesis H_0 and its alternative hypothesis H_a :

$$H_0 : R(f^0) - R(f_{\mathcal{W}_M}^0) = 0, \quad H_a : R(f^0) - R(f_{\mathcal{W}_M}^0) < 0, \quad (5)$$

where R represents the risk under the data distribution, and f^0 and $f_{\mathcal{W}_M}^0$ are two population risk minimizers of decision functions on all words \mathcal{W} and those with masked words of \mathcal{W} , respectively. The masked words of \mathcal{W} are those highly attended words of \mathcal{W} by transformer-based models such as BERT [9] on training samples. It is important to note that masking highly attended words of \mathcal{W} is crucial since state-of-the-art embedding models such as BERT can infer words that other embedding models such as Word2Vec [32] are incapable of. For more details, refer to Section VI-B.

¹Given that the knowledge is unknown concerning the performance of a candidate generator over the PASS generator, we perform a two-sided test to avoid Type-III error.

Algorithm 2: PAI: Sentiment Word Inference

Input : Words of interest \mathcal{W}_M ; Pre-trained transformer encoder \mathcal{E} ; Attention threshold $\delta \in (0, 1)$; Inference sample \mathbb{S} ; PASS generator \mathcal{G}_h on embeddings; MC size D .

Output : A P-value indicating whether \mathcal{W}_M contributes to classification by testing (5).

```

// Create an inference sample masked by  $\mathcal{W}_M$ 
1 for every sequence  $\mathbf{z} = (z_t)_{t=1}^T$  in  $\mathbb{S}$  do
2   for every token  $z_t$  in  $\mathbf{z}$  do
3     Use  $\mathcal{E}$  to extract attention weights of all other
4     tokens in  $\mathbf{z}$ , attended by  $z_t$ ;
5     Mask  $\delta$  proportion of all other tokens starting
6     from those with small attention weights;
7     Collect the masked sequence  $\mathbf{z}_M$ .
8   end
9 end
10 Get the masked inference sample  $\mathbb{S}_M$  from  $\mathbf{z}_M$ . Then
    apply  $\mathcal{E}$  to inference samples  $\mathbb{S}$  and  $\mathbb{S}_M$ , and get
    embedded inference samples  $\mathbb{E}$  and  $\mathbb{E}_M$ .
// Calculate test statistic with embeddings
11 Compute  $T$  using (6) on  $\mathbb{E}$  and  $\mathbb{E}_M$ .
// Estimate the distribution of  $T$  under  $H_0$ 
12 for  $d = 1, \dots, D$  do
13   Generate  $\mathbb{E}^{(d)}$  of size  $|\mathbb{E}|$  using  $\mathcal{G}_h$ ;
14   Compute  $T^{(d)}$  on  $\mathbb{E}^{(d)}$  using (6).
15 end
16 Obtain  $F_D$ , the empirical CDF of  $(T^{(d)})_{d=1}^D$ .
17 return P-value =  $F_D(T)$ .
```

PAI constructs a test statistic T using the empirical risk R_n evaluated on an inference sample that is independent of the training sample:

$$T = \frac{R_n(\hat{f}) - R_n(\hat{f}_{\mathcal{W}_M})}{SE(R_n(\hat{f}) - R_n(\hat{f}_{\mathcal{W}_M}))}, \quad (6)$$

where \hat{f} and $\hat{f}_{\mathcal{W}_M}$ are the corresponding trained decision functions, R_n is the empirical risk evaluated on an independent inference sample, and $SE(\cdot)$ denotes the standard error.

For sentiment analysis, we further split the inference sample \mathbb{S} into training and test sets for training and evaluating a classifier, as in Section V-A. Then, we proceed in three steps. First, we train normalizing flows on \mathbb{S}_h to generate the joint null distribution of masked embeddings and sentiment labels under H_0 . Second, we train sentiment classifiers \hat{f} and $\hat{f}_{\mathcal{W}_M}$ respectively on the training set and its masked version to get test statistic (6). Third, we generate D datasets on the embedding space $\mathbb{E}^{(d)} = (\mathbf{X}_i^{(d)}, Y_i^{(d)})_{i=1}^n$ from the null distribution estimated by PASS to compute corresponding test statistics $(T^{(d)})_{d=1}^D$ on the test set to obtain the empirical null distribution of T , where $\mathbf{X}_i^{(d)}$ and $Y_i^{(d)}$ represent embedding and corresponding sentiment label, $T^{(d)} = \bar{R}^{(d)} / SE(\bar{R}^{(d)})$ and $\bar{R}^{(d)} = R_n(\hat{f}^{(d)}) - R_n(\hat{f}_{\mathcal{W}_M}^{(d)})$ are calculated on $\mathbb{S}^{(d)}$. Finally, we obtain the P-value of T evaluated on the test set by comparing its value with the empirical distribution of

$(T^{(d)})_{d=1}^D$, c.f., Algorithm 2 for details.

Next, we perform an error analysis for estimating the data distribution F_Z by a coupling flow $F_Z = F_V(\tilde{G}^{-1})$ in the Hellinger-distance $h(\tilde{F}_Z, F_Z) = \frac{1}{2} \int (\sqrt{\tilde{p}_Z} - \sqrt{p_Z})^2 d\mu$ is between \tilde{F}_Z and the true distribution F_Z , where \tilde{p}_Z and p_Z are probability densities with respect to the measure μ . On this ground, we provide a guarantee of the PAI test's validity in (4).

C. Text-to-Image Generation

Stable Diffusion, a latent diffusion model [38], can generate detailed images given a text prompt. This subsection performs a conditional inference to quantify the statistical certainty of text-to-image generation. Given two text prompts $\mathbf{x}^{(1)}$ and $\mathbf{x}^{(2)}$, we construct a coherence test for corresponding generated images $\mathbf{Y}^{(1)}$ and $\mathbf{Y}^{(2)}$ by contrasting their conditional distributions $P(\mathbf{y}|\mathbf{x}^{(1)})$ and $P(\mathbf{y}|\mathbf{x}^{(2)})$.

For uncertainty quantification, we use the Inception-V3 embeddings $\mathbf{e}^{(k)}$ [47] for images $\mathbf{Y}^{(k)}$; $k = 1, 2$. Under the Gaussian assumption [18], we define the FID score $\text{FID}(P_1, P_2)$ between the distributions of two embeddings $\mathbf{e}^{(k)}$; $k = 1, 2$, as a coherence measure for hypothesis testing:

$$H_0 : \text{FID}(P_1, P_2) = 0, \quad H_a : \text{FID}(P_1, P_2) > 0. \quad (7)$$

Moreover, we construct $T = \text{FID}(\hat{P}_1, \hat{P}_2)$ as a test statistic, where \hat{P}_k is the corresponding empirical distribution of image embeddings on an inference sample of size n_k ; $k = 1, 2$.

For PAI inference, we use pre-trained Stable Diffusion model [38], a state-of-the-art text-to-image generative model, as our PASS generator. Then, we apply PASS to simulate the null distribution of test statistic T . Given prompt $\mathbf{x}^{(k)}$, for $d = 1, \dots, D$, PASS generates synthetic samples from P_k , resulting in synthetic embeddings $(\mathbf{e}_i^{(k)})_{i=1}^{n_1+n_2}$, of which $(\mathbf{e}_i^{(k)})_{i=1}^{n_1}$ and $(\mathbf{e}_i^{(k)})_{i=n_1+1}^{n_1+n_2}$ are used to calculate FID score $T_k^{(d)}$, which then renders a sample of the test statistic $(T_d^{(k)})_{k=1,2;d=1,\dots,D}$ of size $2D$, under the null hypothesis. Under the null that $P_1 = P_2$, there is no difference between the distribution of $\mathbf{e}_i^{(1)}$ and that of $\mathbf{e}_j^{(2)}$, and thus $T_k^{(d)}$ would be a good estimate for the FID score under H_0 , using synthetic samples from PASS. Additionally, $T_k^{(d)}$ also accounts for the symmetry between P_1 and P_2 when calculating FID score. By randomly mixing them, we obtain an estimated null distribution for T ; c.f., Algorithm 3 for details.

VI. NUMERICAL RESULTS

A. Image synthesis

This subsection applies PAI in Section V to hypothesis testing (4) on the quality of image synthesis using the CIFAR-10 benchmark [28]. This dataset consists of 60,000 images of size $(3 \times 32 \times 32)$ in 10 different classes, with 50,000 training and 10,000 test images.

To synthesize images, we use the CIFAR-10 training set while we use a randomly selected subset of size n of the CIFAR-10 test set for inference. Additionally, we split the CIFAR-10 training set equally into a holdout sample of size $n_h = 25,000$ and another sample of size $n_t = 25,000$, respectively for training a PASS generator (reference) and

Algorithm 3: PAI: Multimodal Inference

Input : Two sets of image embeddings \mathbb{S}_1 and \mathbb{S}_2 generated from two prompts $\mathbf{x}^{(1)}$ and $\mathbf{x}^{(2)}$; PASS generator \mathcal{G}_h ; MC size D .
Output : A P-value indicating whether $\mathbf{x}^{(1)}$ and $\mathbf{x}^{(2)}$ generate similar images by testing (7).

```

// Calculate the test statistic
1 Compute  $T = \text{FID}(\hat{P}_1, \hat{P}_2)$  where  $\hat{P}_1$  and  $\hat{P}_2$  are empirical distributions of  $\mathbb{S}_1$  and  $\mathbb{S}_2$ .
// Estimate the distribution of  $T$  under  $H_0$ 
2 for  $k = 1, 2$  do
3   for  $d = 1, \dots, D$  do
4     Generate  $\mathbb{S}_1^{(d)}$  of size  $|\mathbb{S}_1|$  and  $\mathbb{S}_2^{(d)}$  of size  $|\mathbb{S}_2|$  using  $\mathcal{G}_h$  given prompt  $\mathbf{x}^{(k)}$ ;
5     Compute  $T_k^{(d)} = \text{FID}(\hat{P}_1^{(d)}, \hat{P}_2^{(d)})$ , where  $\hat{P}_1^{(d)}$  and  $\hat{P}_2^{(d)}$  are the empirical distributions of  $\mathbb{S}_1^{(d)}$  and  $\mathbb{S}_2^{(d)}$ , respectively.
6   end
7 end
8 Get  $F_D$ , the empirical CDF of  $(T_1^{(d)})_{d=1}^D \cup (T_2^{(d)})_{d=1}^D$ .
9 return P-value =  $1 - F_D(T)$ .
```

training competitor generators. In (1), we use a diffusion model (DDPM, [19]) as our baseline generator, denoted by PASS-DDPM. We compare the FID scores of three candidate generators against the baseline generator PASS-DDPM, including DDPM, deep convolutional GAN (DCGAN, [35]), and generative flow (GLOW, [24]); see Fig 2 for samples of the generated images by these generators. To compute the FID scores, we use a 2048-dimensional feature map extracted from an intermediate layer of a pre-trained Inception-V3 model [47] on generated images.

For the hypothesis test in (5), we use PASS-DDPM with $D = 500$ to estimate the null distribution of the FID score and then compute the corresponding P-value for an inference sample, as shown in Table I. Fig 3 illustrates that the empirical null distribution of the FID score varies with the inference sample size n and becomes more concentrated as n increases. This observation highlights the importance of performing uncertainty quantification for the FID score since relying solely on the numerical score could be misleading. Furthermore, we find that DDPM, a generator similar to PASS-DDPM, has a P-value of .78, indicating no significant deviation from the baseline PASS-DDPM. However, DCGAN and GLOW exhibit substantial differences from PASS-DDPM, with P-values of .00 at a significance level of $\alpha = .05$. We confirm this conclusion as the inference sample size increases from $n = 2,050$ to $n = 10,000$.

The experiment result shows that DDPM generators are comparable to the baseline PASS-DDPM, but DCGAN and GLOW show significant differences. It underscores the need to account for uncertainty in the FID score to avoid drawing incorrect conclusions about the generation performance.

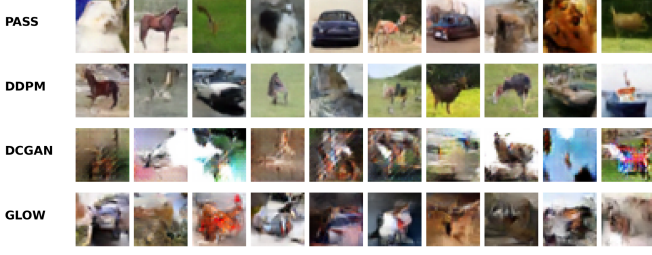


Fig. 2. Generated fake CIFAR10 images (32, 32) using PASS-DDPM, DDPM, DCGAN, and GLOW, based on 25,000 training images from top to bottom.

TABLE I

FID SCORES AND THEIR P-VALUES FOR TESTING (4), COMPARING THREE GENERATORS, DDPM, DCGAN AND GLOW, AGAINST THE BASELINE PASS-DDPM. HERE FID SCORES ARE COMPUTED ON 2048-DIMENSIONAL FEATURE MAPS OF INCEPTION-V3 MODEL [47] WITH n TEST AND n SYNTHESIZED IMAGES, AND DIST-AVG DENOTES THE AVERAGE FID SCORES OF PASS-DDPM.

Inf size/Generator		DDPM	DCGAN	GLOW	DIST-AVG
$n = 2,050$	FID	49.55	92.93	76.37	49.75
	P-value	.78	.00	.00	
$n = 5,000$	FID	36.83	80.11	64.32	37.04
	P-value	.65	.00	.00	
$n = 10,000$	FID	32.57	76.17	61.01	32.58
	P-value	.72	.00	.00	

B. Sentiment Word Inference

This subsection applies PAI to construct a significance test for quantifying the relevance of sentiment collections of positive, negative, and neutral words, in the context of sentiment classification on the IMDB benchmark [30]. This dataset comprises 50,000 movie reviews labeled as positive or negative. The goal is to determine whether each collection of words contributes significantly to sentiment analysis.

To perform sentiment analysis, we use a pre-trained DistilBERT model [40] to generate text embeddings. Then, we estimate the null distribution of a test statistic using a normalizing flow with a holdout sample of size $n_h = 35,000$, followed by the test (4) in Section V-B with an inference sample of size $n = 5,000$ with a sentiment classifier trained on an independent training set of size 10,000.

Extraction of Sentiment Words. We extract positive and negative sentiment words of IMDB reviews while treating any remaining words as neutral words based on the opinion lexicon provided by [22]. Then, we extract $|W_M| = 600$ most frequent positive and negative, and neutral words in each collection for inference. Table II displays subsets of these words.

Masking Contexts of Sentiment Words. One main challenge is that BERT-like models [9] have the capability of inferring the context information of sentences via unmarked words due to the use of masked-language modeling for training. As a result, simply masking uni-gram sentiment words does not impact sentiment analysis. To solve this issue, we propose to mask the context of each target word by thresholding attention weights from a pre-trained transformer encoder such that 2% of the context words are masked.

Training via Transfer Learning. To perform sentiment analysis, we construct a classifier by appending a classification

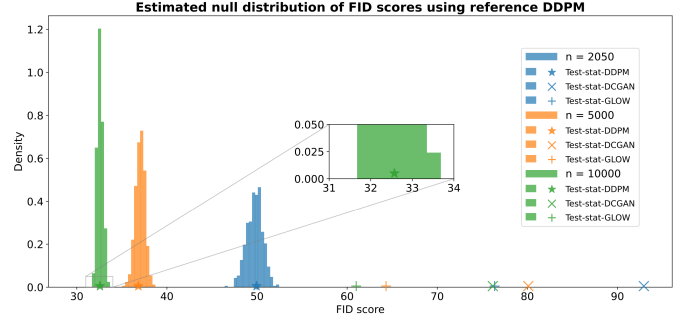


Fig. 3. Empirical FID score distributions with inference sizes $n = 2050, 5000, 10,000$ based on $D = 500$ PASS samples from our PASS-DDPM, represented by colors blue, orange, and green. The FID score is computed using 2048-dimensional features extracted from the Inception-V3 model [47].

head to a pre-trained uncased base DistilBERT model [40], a lighter version of BERT, which permits efficient comprehending of the context. We then fine-tune the model using IMDB review data and obtain fine-tuned embeddings for subsequent tasks. As a result, the model achieves high test accuracy with only a few epochs of fine-tuning.

Learning Embedding Distribution by Normalizing Flows. To train a PASS on the embedding space, we train a RealNVP [12] with affine coupling layer on an independent holdout sample $n_h = 35,000$ to learn the joint distribution of the pair of text embedding and sentiment label. Specifically, we first learn the marginal distribution of sentiment labels and then use normalizing flows to learn the conditional distribution of text embeddings given a sentiment label. The learned flow will be used to emulate the null distribution of the test statistic. We refer to A2 of the Appendix for more training details. As Fig 4 suggests, PASS produces an accurate joint null distribution of the word-label pair, evident from the corresponding marginal and conditional distributions given the label.

PAI. We apply PASS to generate $D = 200$ synthetic samples from the null distribution learned from the normalizing flows. Then, we use a training sample of size $n_t = 10,000$ to train a classification model while computing the test statistic on the inference sample of size $n = 5,000$, with the same splitting ratio for all synthetic samples.

TABLE II

DEGREE OF IMPORTANCE OF THREE COLLECTIONS OF 600 OF POSITIVE, NEGATIVE, NEUTRAL WORDS, AS MEASURED BY THE P-VALUE AGAINST IRRELEVANCE OF EACH COLLECTION BY PAI WITH A MC SIZE $D = 200$.

	Selected sentiment words	P-value
Positive	"gratitude, radiant, timely, robust, optimal, thoughtfully, cooperative, calming, assurance, oasis, elegant, remarkable, restored, fantastic, diplomatic, fastest, excellence, precise, brisk, warmly, ..."	.045
Negative	"cringed, vomit, excuse, vomiting, fails, ashamed, boring, limp, ridiculous, aground, scrambled, useless, snarl, annoying, bland, unnatural, incorrectly, dire, idiot, leaking, ..."	.015
Neutral	"administering, reorganized, curving, gleamed, relinquished, circled, seeded, streamed, curved, scholastic, canning, accommodated, voluntary, cooled, rained, defected, regulated, ousted, straightening, renaming, ..."	.715

Table II and Fig 5 show that positive and negative words

have significant P-values of .045 and .015, while neutral words are insignificant with a P-value of .715, at a significance level of $\alpha = .05$. In other words, positive and negative sentiment words, particularly their contexts, are important predictive features for sentiment analysis.

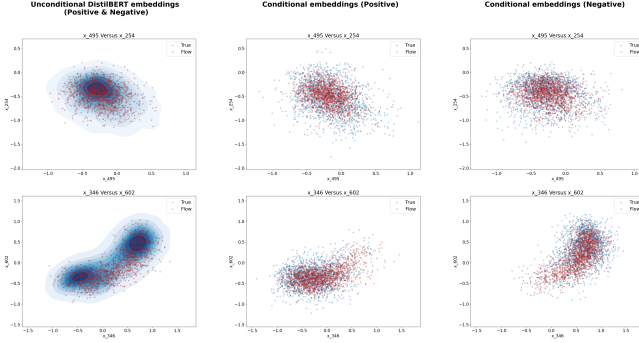


Fig. 4. Two-dimensional projections from null distributions by PASS (blue) from affine coupling flows trained on a holdout sample of size $n_h = 35,000$ versus the true distribution (red) via 768-dimensional DistilBERT embeddings. The marginal distribution of combined words and conditional distributions for positive and negative reviews are from left to right.

To understand the contribution of PASS for simulating the test statistic null distribution, we note that the joint null distribution of positive, neutral, or negative words does not follow the standard Gaussian with an MC size of $D = 200$, as indicated by Table III. Their distributions differ significantly from their asymptotic distributions [5], despite their smooth curves resembling the Gaussian distribution, as shown in Fig 5. As a result, the asymptotic test in [5] is not appropriate in this situation. This result demonstrates the usefulness of PASS when a test statistic’s distribution significantly deviates from its asymptotic distribution.

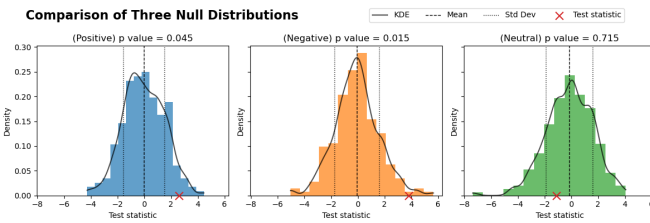


Fig. 5. Empirical null and their kernel smoothed distributions of the test statistic T for positive (blue), negative (orange), and neutral (green) sentiment words, based on PASS with an MC size $D = 200$ for the hypothesis (5). Here, red crosses represent the test statistic’s values calculated on an inference sample, while the dashed line and two dotted lines represent the empirical mean and standard error.

C. Text-to-Image Generation

Consider four prompts as follows: Prompt 1 - “The sun sets behind the mountains”, Prompt 2 - “The sun sets behind the mountains”, Prompt 3 - “The mountains with sunset behind”, and Prompt 4 - “The mountains with a night sky full of shining stars”. The four prompts have different levels of

TABLE III
THE KOLMOGOROV-SMIRNOV TEST FOR THE DISCREPANCY BETWEEN THE TEST STATISTIC’S DISTRIBUTION AND THE STANDARD GAUSSIAN.

	Empirical mean	Std Err	KS test statistic	P-value (two-sided)
Positive	-.028	1.530	.124	.004
Negative	-.083	1.659	.128	.002
Neutral	-.137	1.749	.157	.000

similarities: Prompts 1 and 2 are identical, Prompt 1 (or 2) is similar to Prompt 3, and Prompt 4 differs from all three above, with the Cosine similarity of 1, .891, .590, and .607 in Table IV. Visually, images from Prompts 1 (or 2) and 3 appear very similar with only slight differences, whereas those from Prompt 4 display stars and look dramatically different, as illustrated in Fig 6. Next, we will confirm the visual impressions through our coherence test in (7).



Fig. 6. Generated images given different prompts by Stable Diffusion. The image size is cropped from (512, 512) to (299, 299) to accommodate the input shape for Inception-V3 model [47].

TABLE IV
COMPARISON OF FOUR PAIRS OF PROMPTS WITH THE COSINE SIMILARITY ON THE CLIP TEXT EMBEDDINGS, THE FID SCORE TEST STATISTIC, AND THE P-VALUE BY PASS WITH $D = 200$, ON 192-DIMENSIONAL EMBEDDINGS FROM THE INCEPTION-V3 MODEL.

	Cosine similarity	FID score	P-value
Prompts 1 and 2 (same)	1.000	.544	.990
Prompts 1 and 3 (similar)	.891	1.010	.124
Prompts 1 and 4 (different)	.590	14.250	.000
Prompts 3 and 4 (different)	.607	14.172	.000

To apply PAI for testing in (7), we construct a PASS generator using a pre-trained stable diffusion model to generate two image sets given two prompts. This pre-trained model is a well-trained SOTA (the Self-Organizing Tree Algorithm) text-to-image model (equivalent to $n_h \rightarrow +\infty$). Then, we compute the FID score of 192-dimensional Inception-V3 embeddings between the two sets of images. To simulate the null distribution, we apply PAI to the test statistic with an MC size of $D = 200$ for both image sets, where the effective size of a sample is 400.

Images generated under Prompts 1 and 2, and Prompts 1 and 3, are statistically indistinguishable, given the corresponding P-values of 0.99 and 0.124 at a significance level $\alpha = .05$ in Table IV. In contrast, Prompts 1 and 4; Prompts 3 and 4 significantly differ in image generation as they have different implications. Moreover, we construct more pairs of prompts to obtain a spectrum of cosine similarity versus FID score, along with the corresponding test results. As illustrated in Fig 7, a

small FID score and a large Cosine similarity imply that two prompts are conceptually equivalent or similar, which can be captured by the test under different significance levels.

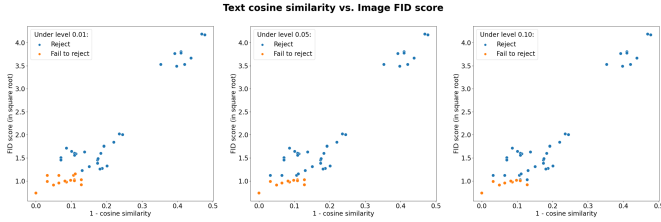


Fig. 7. Pairs of FID score and Cosine similarity on embeddings generated from CLIP versus the FID score (test statistic) computed based on 192-dimensional features from the Inception-V3 model [47], under different significance levels $\alpha = .01, .05, .1$. Each point in the plot represents a pair of prompts.

VII. CONCLUSION

This paper presents a novel generative scheme, PASS, and an inference framework, PAI, developed to facilitate statistical inference from complex and unstructured data such as gene expression, images, and texts. These tools are designed to address the scarcity of effective uncertainty quantification methods in black-box models like deep neural networks.

PASS distinguishes itself by generating synthetic data that aligns closely with the distribution of the raw data. It leverages the capabilities of large pre-trained generative models, such as diffusion models and normalization flows, to boost estimation accuracy. Additionally, the PASS generator enables data integration and personalization via multivariate rank matching on latent variables, while adhering to privacy standards through data perturbation. We theoretically delve into the sampling properties of PASS and confirm that the ranks of the latent variables can be approximated post-data perturbation. Experimental evidence underscores the superior generation quality of PASS.

The PAI framework, built on the foundation of PASS, excels in estimating the distribution of any statistic through Monte Carlo experiments, thus providing a robust method for conducting statistical inference. We theoretically guarantee the inference validity of PAI even when data is scarce. We demonstrated its wide-ranging applications experimentally.

Our primary objective is to equip researchers with tools that aid in deriving reliable and reproducible conclusions from data. These tools have the potential to elevate the credibility and reliability of data-driven discoveries and statistical inference.

VIII. APPENDIX

APPENDIX

A. Training Details

1) *Image Synthesis*: Technical details for training various generative models to learn the distribution of CIFAR-10 data are as follows. We trained using either a single TITAN RTX GPU or multiple GPUs, modifying the source code to accommodate numerical experiments. Here, we have not

optimized tuning parameters for generation quality, as we only use trained models for uncertainty quantification.

- **PASS and DDPM**: To train diffusion models, we adopt the code `Denoising-Diffusion`² using the Adam optimizer with a learning rate of 8×10^{-5} , 4×10^5 time steps, a batch size of 32, and 250 sampling time steps using a light-weight fast sampler DDIM [45].
- **DCGAN**: We adopt the implementation of DCGAN-CIFAR10³ using the Adam optimizer with a learning rate of 1×10^{-3} , a batch size of 128, and 30 epochs. Both the generator and discriminator are CNNs and are trained alternatively.
- **GLOW**: We implement using `Glow-PyTorch`⁴. Specifically, we train the GLOW model with its default normalizing flow structure using an additive coupling layer and the Adamax optimizer with a learning rate of 5×10^{-4} , weight decay of 5×10^{-5} , a batch size of 64, and 250 epochs.

2) *Sentiment Word Inference*: We provide details about training the sentiment classifier and normalizing flows.

- **Sentiment Classifier**. We fine-tuned a pre-trained DistilBERT model from the `transformers` library⁵ by attaching a classification head, where we fine-tuned for five epochs with an Adam optimizer using a learning rate of 10^{-5} and default exponential decay rates.
- **Normalizing Flows**. We trained normalizing flows to learn the null distribution using a RealNVP architecture with ten affine coupling layers, with batch normalization and reverse permutation layers in between. We learned each affine coupling layer's parameters using a ReLU neural network with three hidden layers with dimensions 8192, 4096, and 2048. The model was implemented using the `pyro` framework⁶. The normalizing flow model was trained using an Adam optimizer with a learning rate of 7×10^{-5} and default exponential decay rates. The batch size was set to 64, and we used a linear one-cycle learning rate scheduler [43] for 500 epochs to avoid overfitting while allowing for warm starting. The training process also involved monitoring the generated embeddings versus true embeddings for selected coordinate pairs.

All training processes, including DistilBERT's fine-tuning and full training of normalizing flows, are performed on 4 TITAN RTX GPUs with mixed precision.

3) *Text-to-Image Generation*: For a text-to-image generator, we use the pre-trained stable diffusion model v1-4 hosted on HuggingFace⁷, with 50 inference steps and guidance scale as 2. To calculate the FID score, we utilize the implementation from `torchmetrics`⁸, which uses pre-trained Inception-V3 model [18] for extracting image embeddings. The experiment is performed on 8 TITAN RTX GPUs with mixed precision.

²DDPM: <https://github.com/lucidrains/denoising-diffusion-pytorch>

³DCGAN: <https://github.com/Amaranth819/DCGAN-CIFAR10-Pytorch>

⁴Glow-PyTorch: <https://github.com/y0ast/Glow-PyTorch>

⁵transformers: <https://github.com/huggingface/transformers>

⁶pyro: <https://github.com/pyro-ppl/pyro>

⁷stable-diffusion: <https://huggingface.co/CompVis/stable-diffusion>

⁸torchmetrics: <https://github.com/Lightning-AI/torchmetrics>

B. Multivariate Rank

We now discuss the optimal transportation approach to define ranks for a random vector, referred to as *multivariate ranks* [7], which generalizes the concept of univariate rank. First, we introduce some notations: for two probability measures μ and ν on \mathcal{R}^d , and a function $F : \mathcal{R}^d \rightarrow \mathcal{R}^d$, if for any $\mathbf{X} \sim \mu$, $F(\mathbf{X}) \sim \nu$, we say F pushes μ to ν , denoted as $F\#\mu = \nu$. Here we use $P(\mathcal{R}^d)$ and \mathcal{U}^d to denote the set of all probability measures defined on \mathcal{R}^d and for the uniform measure on $[0, 1]^d$.

Definition 1 (Population Rank Map). *For any $\mu \in P(\mathcal{R}^d)$, the map $R : \mathcal{R}^d \rightarrow [0, 1]^d$ is the rank map of μ if (i) $R\#\mu = \mathcal{U}^d$ and (ii) $R = \nabla\Psi$ for some real-valued convex function Ψ on \mathcal{R}^d .*

Remark 4. Requirement (ii) in Definition 1 ensures, but is not limited to, the monotonicity property of the map. For example, in the univariate case, if $x < y$, then it is natural to expect their ranks to satisfy $R(x) < R(y)$. In the multivariate case, we do not have a canonical ordering, but (ii) implies that $R(\cdot)$ is cyclically monotone [37], which is a generalization of univariate monotonicity.

The rank map $R(\cdot)$ is well-defined by McCann’s Theorem ([7], [31], [48]). Moreover, if μ has a finite second moment, then $R(\cdot)$ is also the solution of *Monge’s problem* $\inf_{F: F\#P=Q} \int c(\mathbf{x}, F(\mathbf{x}))dP$ with $P = \mu$, $Q = \mathcal{U}^d$, and $c(\mathbf{y}, \mathbf{z}) = \|\mathbf{y} - \mathbf{z}\|^2$. Note that the rank map reduces to the CDF of the measure μ when $d = 1$ but is generally not analytically tractable when $d > 1$ except for some special cases. In practice, we estimate the population rank map via a random sample.

Definition 2 (Empirical Rank Map). *Denote $\mathbf{h}_1^d, \dots, \mathbf{h}_n^d$ as a d -dimensional Halton sequence with ν_n as its empirical measure. Let μ_n be the empirical measure based on $\mathbf{Y}_1, \dots, \mathbf{Y}_n$. Then, the map $R_n^Y : (\mathbf{Y}_i)_{i=1}^n \rightarrow (\mathbf{h}_i^d)_{i=1}^n$ obtained by solving Monge’s problem with $P = \mu_n$ and $Q = \nu_n$, is called the empirical rank map of $(\mathbf{Y}_i)_{i=1}^n$.*

Remark 5. The Halton sequence [1] is a fixed sequence in $[0, 1]^d$ whose empirical measure converges weakly to the uniform distribution $U[0, 1]^d$. This sequence is the multivariate ranks in \mathcal{R}^d .

The computation of empirical ranks R_n^Y amounts to solving the discrete Monge’s problem, or identifying a permutation map $\pi_* = \arg \min_{\pi} \sum_{i=1}^n \|\mathbf{Y}_{\pi(i)} - \mathbf{h}_i^d\|_2^2$ over all permutation maps π on $\{1, \dots, n\}$. Then, $R_n^Y(\mathbf{Y}_{\pi_*(i)}) = \mathbf{h}_i^d$. In the case of $d = 1$, we choose $h_i^1 = \frac{i}{n}$; $i = 1, \dots, n$, and the empirical rank map R_n^Y coincides with the univariate rank up to a constant.

Rank matching in PASS. The empirical ranks provides a distribution-free way to measure the closeness between two multivariate samples in terms of their ranks. This property motivates the approximate rank matching in (1) for PASS. To determine a permutation map $r = \pi_2 \circ \pi_1^{-1}$ matching the empirical ranks of $(\mathbf{U}_{r(i)})_{i=1}^n$ to those of $(T(\mathbf{Z}_i))_{i=1}^n$, we compute the permutation map $\pi_1(\cdot)$ by minimizing $\sum_{i=1}^n \|T(\mathbf{Z}_{\pi(i)}) - \mathbf{h}_i^d\|_2^2$ and $\pi_2(\cdot)$ by minimizing $\sum_{i=1}^n \|\mathbf{U}_{\pi(i)} - \mathbf{h}_i^d\|_2^2$.

Algorithm 4: Multivariate rank matching

Input : Latent representations $(T(\mathbf{Z}_i))_{i=1}^n; (\mathbf{U}_i)_{i=1}^n$.
Output : A permutation map r that matches the ranks of $(\mathbf{U}_{r(i)})_{i=1}^n$ and those of $(T(\mathbf{Z}_i))_{i=1}^n$.

- 1 Compute the permutation map $\pi_1(\cdot)$ by minimizing $\sum_{i=1}^n \|T(\mathbf{Z}_{\pi(i)}) - \mathbf{h}_i^d\|_2^2$ over all permutation maps;
- 2 Compute the permutation map $\pi_2(\cdot)$ by minimizing $\sum_{i=1}^n \|\mathbf{U}_{\pi(i)} - \mathbf{h}_i^d\|_2^2$ over all permutation maps;
- 3 **return** $r = \pi_2 \circ \pi_1^{-1}$.

Computation complexity. The computational complexity for $r(\cdot)$ boils down to solving a balanced linear sum assignment problem (LSAP) with cost matrix $\mathbf{C} = (C_{ij})_{n \times n}$, where $C_{ij} = n^{-1} \|\mathbf{Y}_i - \mathbf{h}_j^d\|_2^2$. This problem can be solved using the Hungarian algorithm [23]. When $n \gg d$, the complexity of matching multivariate ranks in (1) is $O(n^3)$ as many variants of the Hungarian algorithm admit a worst-case complexity of $O(n^3)$.

C. Rank-Preserving Perturbation Function

In (1), we consider a specific type of perturbation function W to approximately preserve the multivariate ranks of $(T(\mathbf{Z}_i))_{i=1}^n$, that is, $(\mathbf{V}_i)_{i=1}^n$ and $(T(\mathbf{Z}_i))_{i=1}^n$ share similar multivariate ranks. Specifically, $\mathbf{V}_i = W(\mathbf{U}_{r(i)} + \mathbf{e}_i)$ in (1), where W is the optimal transport map from $F_{\tilde{\mathbf{U}}} \equiv F_{\mathbf{U}} \otimes F_{\mathbf{e}}$ to $F_{\mathbf{U}}$, which is the solution to Monge’s problem, and $\mathbf{e}_i = \tau \boldsymbol{\epsilon}_i$, and $\tau > 0$ is the perturbation size and $\boldsymbol{\epsilon}_i \sim F_{\mathbf{e}}$ is a standardized noise distribution. Note that by (1), $\mathbf{V}, \mathbf{U}, T(\mathbf{Z}) \sim F_{\mathbf{U}}$, and thus we do not distinguish between $F_{\mathbf{V}}, F_{T(\mathbf{Z})}$ and $F_{\mathbf{U}}$. As indicated by Theorem 3, W achieves the desired goal to rank preservation.

To proceed, denote $f(\tau) = \sup_{\mathbf{z} \in \mathcal{Z}} \|R(\mathbf{z}) - \tilde{R}(\mathbf{z})\|^2$ as the discrepancy between base distribution $F_{\mathbf{U}}$ and linearly perturbed distribution $F_{\tilde{\mathbf{U}}}$, where R and \tilde{R} are the corresponding population rank maps. Let $\mathbf{R}^V = [\mathbf{R}_1^V, \dots, \mathbf{R}_n^V]$ and $\mathbf{R}^T = [\mathbf{R}_1^T, \dots, \mathbf{R}_n^T]$ be the multivariate ranks of $(\mathbf{V}_i)_{i=1}^n$ and those of $(T(\mathbf{Z}_i))_{i=1}^n$, respectively. \mathbb{J}_g stands for the Jacobian of a function g . Define $\|\mathbf{R}^V - \mathbf{R}^T\|_n = \left(n^{-1} \sum_{i=1}^n \|\mathbf{R}_i^V - \mathbf{R}_i^T\|_2^2 \right)^{1/2}$. Let the perturbed base vector $\tilde{\mathbf{U}} = \mathbf{U} + \mathbf{e} \sim F_{\tilde{\mathbf{U}}}$. We assume the following conditions:

- (A) (Distribution) $F_{\mathbf{U}}$ and $F_{\tilde{\mathbf{U}}}$ are absolutely continuous on \mathcal{R}^d .
- (B) (Moment) For some $t > 0$, $\alpha > 0$ and $\tau_0 > 0$, $E[\exp(t\|\mathbf{U}\|^\alpha)] < \infty$ and $\sup_{\tau \in [0, \tau_0]} E[\exp(t\|\tilde{\mathbf{U}}\|^\alpha)] < \infty$.
- (C) (Lipschitz) Population rank maps R and \tilde{R} are L -Lipschitz continuous.
- (D) (Commutability) $J_W(\tilde{\mathbf{U}})J_R(W(\tilde{\mathbf{U}})) = J_R(W(\tilde{\mathbf{U}}))J_W(\tilde{\mathbf{U}})$ almost surely.

Theorem 3 (Rank-preservation perturbation). *Under Assumptions (A)-(D), for $d \geq 1$,*

$$\|\mathbf{R}^V - \mathbf{R}^T\|_n^2 = O_p \left(\max \left(r_{n,d} (\log n)^{t_{\alpha,d}}, \tau^2 n^{-1/2} + f(\tau) \right) \right),$$

where $r_{n,d} = n^{-1}$ and $t_{\alpha,d} = 0$ when $d = 1$; $r_{n,d} = n^{-1/2}$ and $t_{\alpha,d} = (4\alpha)^{-1}(4 + 0 \vee (2\alpha + 2d\alpha - d))$ when $d = 2, 3$ and $t_{\alpha,d} = \alpha^{-1} \vee (7/2)$ when $d = 4$; $r_{n,d} = n^{-1/d}$ and $t_{\alpha,d} = 2(1 + d^{-1})$ when $d \geq 5$.

Proof of Theorem 3: Note that

$$\|\mathbf{R}^V - \mathbf{R}^T\|_n^2 \leq 2\|\mathbf{R}^V - \tilde{\mathbf{R}}\|_n^2 + 2\|\tilde{\mathbf{R}} - \mathbf{R}^T\|_n^2, \quad (8)$$

where $\tilde{\mathbf{R}} = [\tilde{\mathbf{R}}_1, \dots, \tilde{\mathbf{R}}_n]$ are the empirical ranks of perturbed samples $(\tilde{\mathbf{U}}_i)_{i=1}^n$ with $\tilde{\mathbf{U}}_i = \mathbf{U}_{r(i)} + \mathbf{e}_i$. Hence, the desired result follows by applying Lemma 2 to the first term on the RHS of (8), and Lemma 3 to the second one by noticing that \mathbf{R}^T are also empirical ranks of $(\mathbf{U}_{r(i)})_{i=1}^n$. \square

Theorem 3 suggests that $(\mathbf{V}_i)_{i=1}^n$ preserves the multivariate ranks of $(T(\mathbf{Z}_i))_{i=1}^n$ when $n \rightarrow \infty$, $\tau \rightarrow 0^+$ and $f(\tau) \rightarrow 0$ as $\tau \rightarrow 0^+$. An illustrative example for W that satisfies Assumptions (A)-(D) is provided next.

Example 1. Let $F_U = \otimes_{j=1}^d F_j$ and $F_{\tilde{U}} = \otimes_{j=1}^d \tilde{F}_j$. Assume that F_j and \tilde{F}_j have marginal densities f_j and \tilde{f}_j satisfying $\max_{j=1,\dots,d}(\|f_j \vee \tilde{f}_j\|_\infty) \leq L$. By McCann's Theorem ([7], [31], [48]), $R = (F_1, \dots, F_d)^\top$, $\tilde{R} = (\tilde{F}_1, \dots, \tilde{F}_d)^\top$ and $W = (F_1^{-1} \circ \tilde{F}_1, \dots, F_d^{-1} \circ \tilde{F}_d)$. Then, it is easy to see that Assumptions (A) and (C) hold. Assumption (B) holds if each F_j and \tilde{F}_j admit finite moment generating functions of order $\alpha > 0$. As for Assumption (D), it holds automatically since both \mathbb{J}_W and \mathbb{J}_R are diagonal. Finally, one can show that $f(\tau) \leq L^2 \tau^2 \mathbb{E}\|\epsilon\|^2$ which goes to 0 if we choose $\tau = \tau_n = o(n^{-1/2})$. Note that this example motivates many choices of F_U and F_ϵ . For example, we can choose $F_U = \mathcal{U}^d$ and $F_\epsilon = N(\mathbf{0}_d, \mathbf{I}_d)$.

D. Technical Lemmas for Proving Theorem 3

Lemma 2 (Rank Preservation). *Under Assumptions (A)-(D), the optimal transport map W exactly preserves the population ranks of $(\tilde{\mathbf{U}}_i)_{i=1}^n$, almost surely under $F_{\tilde{U}}$. Furthermore, $(\mathbf{V}_i)_{i=1}^n$ approximately preserves the empirical ranks of $(\tilde{\mathbf{U}}_i)_{i=1}^n$. That is, $\|\mathbf{R}^V - \tilde{\mathbf{R}}\|_n^2 = O_p(r_{n,d}^* (\log n)^{t_{\alpha,d}})$, where $r_{n,1}^* = 0$, and $r_{n,d}^* = r_{n,d}$ when $d > 1$.*

Proof of Lemma 2: To demonstrate the preservation of population ranks, note that R and W are the optimal transportation maps. By the Brenier-McCann Theorem, see Theorem 2.2 of [16], $R = \nabla \Phi_1$ and $W = \nabla \Phi_2$ for some real-valued convex functions Φ_1 and Φ_2 on \mathcal{R}^d under Assumptions (A). Thus, \mathbb{J}_R and \mathbb{J}_W are positive semidefinite. By the chain rule and Assumption (D),

$$J_{R \circ W}(\tilde{\mathbf{U}}) = J_{R \circ W}(\tilde{\mathbf{U}})^\top,$$

almost surely, which implies that $R \circ W$ is the gradient of some real-valued function Φ , i.e., $R \circ W = \nabla \Phi$. Moreover, since both \mathbb{J}_R and \mathbb{J}_W are symmetric and positive semidefinite, we know that $\mathbb{J}_{R \circ W}(\tilde{\mathbf{U}})$, or the Hessian of Φ , is also positive semidefinite. To this end, we conclude that Φ is a convex function, and by the Brenier-McCann Theorem, $R \circ W(\tilde{\mathbf{U}}) = \tilde{\mathbf{R}}(\tilde{\mathbf{U}})$, almost surely, meaning that population ranks of $(\mathbf{V}_i)_{i=1}^n$ are exactly the same as those of $(\tilde{\mathbf{U}}_i)_{i=1}^n$.

Next, we work on preservation of empirical ranks by bounding $\|\mathbf{R}^V - \tilde{\mathbf{R}}\|_n^2$. When $d = 1$, the definition of multivariate ranks coincides with the univariate ranks by a normalizing constant. By definition, the ranks of $(\mathbf{V}_i)_{i=1}^n$ are exactly the same as those of $(\tilde{\mathbf{U}}_i)_{i=1}^n$ since $W = F_U^{-1} \circ F_{\tilde{U}}$, the optimal transport that pushes $F_{\tilde{U}}$ to F_U , is increasing, resulting $\|\mathbf{R}^V - \tilde{\mathbf{R}}\|_n^2 = 0$. For the rest of the proof, we focus on the case of $d \geq 2$. Note that $\|\mathbf{R}^V - \tilde{\mathbf{R}}\|_n^2$ is bounded by

$$C_1 n^{-1} \sum_{i=1}^n \|\mathbf{R}_i^V - R(\mathbf{V}_i)\|^2 + C_2 n^{-1} \sum_{i=1}^n \|R(\mathbf{V}_i) - \tilde{\mathbf{R}}(\tilde{\mathbf{U}}_i)\|^2 + C_3 n^{-1} \sum_{i=1}^n \|\tilde{\mathbf{R}}_i - \tilde{\mathbf{R}}(\tilde{\mathbf{U}}_i)\|^2 \equiv \text{I} + \text{II} + \text{III},$$

where C_1 , C_2 , and C_3 are universal constants. Under Assumptions (A)-(C), by Theorem 2.2 of [6], both I and III are $O_p(r_{n,d} \times (\log n)^{t_{\alpha,d}})$. From the first part of the proof, we have II = 0 almost surely. Then, the desired result follows by combining I, II and III. This completes the proof. \square

Lemma 3 (Stability). *Under Assumptions (A)-(C),*

$$\|\mathbf{R}^T - \tilde{\mathbf{R}}\|_n^2 = O_p(\max(r_{n,d} (\log n)^{t_{\alpha,d}}, \tau^2 n^{-1/2} + f(\tau))).$$

for $d \geq 1$.

Proof of Lemma 3: Note that $\|\mathbf{R}^T - \tilde{\mathbf{R}}\|_n^2$ is bounded by

$$C_1 n^{-1} \sum_{i=1}^n \|\mathbf{R}_i^T - R(\mathbf{U}_{r(i)})\|^2 + C_2 n^{-1} \sum_{i=1}^n \|\tilde{\mathbf{R}}_i - \tilde{\mathbf{R}}(\tilde{\mathbf{U}}_i)\|^2 + C_3 n^{-1} \sum_{i=1}^n \|R(\mathbf{U}_{r(i)}) - \tilde{\mathbf{R}}(\tilde{\mathbf{U}}_i)\|^2 \doteq \text{I} + \text{II} + \text{III}$$

where C_1 , C_2 , and C_3 are all universal constants. Since \mathbf{R}^T are also empirical ranks of $(\mathbf{U}_{r(i)})_{i=1}^n$, we have I = $O_p(r_{n,d} (\log n)^{t_{\alpha,d}})$ due to the consistency⁹ of empirical ranks maps under Assumptions (A)-(C) (Theorem 2.2 of [6]). Similarly, II = $O_p(r_{n,d} (\log n)^{t_{\alpha,d}})$ as well. As for III, note that (up to some constant factors),

$$\begin{aligned} \text{III} &\leq n^{-1} \sum_{i=1}^n \|R(\mathbf{U}_{r(i)}) - \tilde{\mathbf{R}}(\tilde{\mathbf{U}}_i)\|^2 + \\ &\quad n^{-1} \sum_{i=1}^n \|\tilde{\mathbf{R}}(\tilde{\mathbf{U}}_i) - \tilde{\mathbf{R}}(\tilde{\mathbf{U}}_i)\|^2 \\ &\leq L^2 \tau^2 n^{-1} \sum_{i=1}^n \|\epsilon_i\|^2 + \sup_{z \in \mathcal{Z}} \|R(z) - \tilde{\mathbf{R}}(z)\|^2 \\ &= L^2 \tau^2 O_p(n^{-1/2}) + O(f(\tau)). \end{aligned}$$

As a result, III = $O_p(\tau^2 n^{-1/2} + f(\tau))$ with a rate depending on both n and τ . Putting all terms together, we obtain the rate stated in Lemma 3. Moreover, if $f(\tau)$ goes to 0 as $\tau \rightarrow 0^+$ and let $\tau = \tau_n$ to control the rate of convergence for III, which, combined with the rates of I and II, can yield the rate of convergence of $\|\mathbf{R}^T - \tilde{\mathbf{R}}\|_n^2$, as in Lemma 2. This completes the proof. \square

⁹The case when $d = 1$ is not proved in [6] due to simplicity, but it can be easily proved by using Komlós-Major-Tusnády approximation [27] to bound $\|\mathbf{R}^V - \mathbf{R}^T\|_n^2$ directly, resulting in $O_p(n^{-1})$.

E. Technical Proofs of Main Results.

Proof of Lemma 1: Let $T \equiv (T(Z_i))_{i=1}^n$; $\pi_1 \equiv \pi_1(T)$ and $\pi_2 \equiv \pi_2(U)$ be permutation maps in that $T_{\pi_1(i)}$ and $U_{\pi_2(i)}$ have the rank \mathbf{h}_i^d ; $i = 1, \dots, n$, where $(\mathbf{h}_i^d)_{i=1}^n$ denotes the d -dimensional multivariate ranks defined by the Halton sequence, c.f., Appendix B. Then, $r = \pi_2 \circ \pi_1^{-1}$ is the permutation map matching the ranks of $(U_{r(i)})_{i=1}^n$ and $(Z_i)_{i=1}^n$, where $\mathbf{r} = (r_1, \dots, r_n) \in \Pi_n$, the set of all permutations of $(1, \dots, n)$. For any $\mathbf{x}, \mathbf{z} \in \mathcal{R}^d$, $\mathbf{z} \leq \mathbf{x}$ means $z_j \leq x_j$; $j = 1, \dots, d$. Moreover, for convenience, denote $\Pr(\prod_{i=1}^m \{\mathbf{X}_i \leq \mathbf{x}_i\})$ as $\Pr(\mathbf{X}_1 \leq \mathbf{x}_1, \dots, \mathbf{X}_m \leq \mathbf{x}_m)$ for random vectors $(\mathbf{X}_i)_{i=1}^m$ (not necessarily independent nor identically distributed), and fixed points $(\mathbf{x}_i)_{i=1}^m \subset \mathcal{R}^d$.

Part (1): By (1), we show that $(U_{r(i)})_{i=1}^n$ is i.i.d. following F_U . Note that $(\pi_j(1), \dots, \pi_j(n))$ and $(r(1), \dots, r(n))$ are uniformly distributed over Π_n ; $j = 1, 2$. For any $(\mathbf{u}_j)_{j=1}^n \subset \mathcal{R}^d$, $\Pr(\prod_{j=1}^n \{\mathbf{U}_{r(j)} \leq \mathbf{u}_j\})$ is $(n!)^{-1} \sum_{\mathbf{r} \in \Pi_n} \Pr(\prod_{j=1}^n \{\mathbf{U}_{r(j)} \leq \mathbf{u}_j\} | \pi_1 = \mathbf{r})$ since $\Pr(\pi_1 = \mathbf{r}) = (n!)^{-1}$. Note that $r(j) = \pi_2 \circ \pi_1^{-1}(j)$. By Proposition 2.1 of [7], $(U_{r(j)})_{j=1}^n$ and π_2 are independent¹⁰, given $\pi_1 = \mathbf{r}$, $\Pr(\prod_{j=1}^n \{\mathbf{U}_{\pi_2 \circ \pi_1^{-1}(j)} \leq \mathbf{u}_j\} | \pi_1 = \mathbf{r})$ equals to $\Pr(\prod_{j=1}^n \{\mathbf{U}_{\pi_2 \circ \pi_1^{-1}(j)} \leq \mathbf{u}_j\} | \pi_1 = \mathbf{r}, \pi_2 = \mathbf{r})$, which is $\Pr(\prod_{j=1}^n \{\mathbf{U}_j \leq \mathbf{u}_j\} | \pi_1 = \mathbf{r}, \pi_2 = \mathbf{r})$. By the independence of $(\mathbf{U}_j)_{j=1}^n$ and π_1 given $\pi_2 = \mathbf{r}$, $\Pr(\prod_{j=1}^n \{\mathbf{U}_j \leq \mathbf{u}_j\} | \pi_1 = \mathbf{r}, \pi_2 = \mathbf{r})$ is $\Pr(\prod_{j=1}^n \{\mathbf{U}_j \leq \mathbf{u}_j\} | \pi_2 = \mathbf{r})$. Hence, $\Pr(\prod_{j=1}^n \{\mathbf{U}_{r(j)} \leq \mathbf{u}_j\})$ is equal to $(n!)^{-1} \sum_{\mathbf{r} \in \Pi_n} \Pr(\prod_{j=1}^n \{\mathbf{U}_j \leq \mathbf{u}_j\} | \pi_2 = \mathbf{r})$, which is $\Pr(\prod_{j=1}^n \{\mathbf{U}_j \leq \mathbf{u}_j\})$ since $\Pr(\pi_2 = \mathbf{r}) = (n!)^{-1}$ for any $\mathbf{r} \in \Pi_n$. This implies that $(U_{r(i)})_{i=1}^n$ is a random sample from F_U , which in turn implies the desired result.

Part (2): Note that $H(\mathbf{Z}') = H(\mathbf{Z}'_1, \dots, \mathbf{Z}'_n)$, where $\mathbf{Z}'_i = \tilde{G}(W(\mathbf{U}_{r(i)}; \mathbf{e}_i))$, $\mathbf{U} = (\mathbf{U}_i)_{i=1}^n$, and $\mathbf{e} = (\mathbf{e}_i)_{i=1}^n$ are random samples from F_U and F_e . Let $\mathbf{X} \stackrel{d}{=} \mathbf{Y}$ denote \mathbf{X} and \mathbf{Y} having the same distribution. Furthermore, \mathbf{Z}' is only related to \mathbf{Z} through $\pi_1 = \pi_1(T(\mathbf{Z}))$. Then, $H(\mathbf{Z}') | \mathbf{Z}$ has the same distribution of $H(\tilde{G}(W(\mathbf{U}_{r(1)}; \mathbf{e}_1)), \dots, \tilde{G}(W(\mathbf{U}_{r(n)}; \mathbf{e}_n))) | \pi_1$, which is $H(\tilde{G}(W(\mathbf{U}_1; \mathbf{e}_1)), \dots, \tilde{G}(W(\mathbf{U}_n; \mathbf{e}_n))) | \pi_1, \mathbf{r} = (1, \dots, n)$ by the conditional independence of $(r(i))_{i=1}^n$ and $(\mathbf{U}_{r(i)})_{i=1}^n$ given \mathbf{Z} , c.f., Proposition 2.1 of [7]. By the permutation invariance property of $H(\cdot)$, it reduces to $H(\tilde{G}(W(\tilde{\mathbf{U}}_1; \tilde{\mathbf{e}}_1)), \dots, \tilde{G}(W(\tilde{\mathbf{U}}_n; \tilde{\mathbf{e}}_n))) \stackrel{d}{=} H(\mathbf{Z}')$ by the result of **Part (1)** that \mathbf{Z}' is i.i.d. from $\tilde{F}_{\mathbf{Z}}$, which is constructed using independent random samples $(\tilde{\mathbf{U}}_i)_{i=1}^n$ from F_U and $(\tilde{\mathbf{e}}_i)_{i=1}^n$ from F_e . Therefore, $H(\mathbf{Z}')$ and \mathbf{Z} are independent. This concludes the proof. \square

Proof of Theorem 1: From (1), $\mathbf{Z}'^{(d)}$ is a conditionally independent sample of size n given \mathbf{Z} following $F_{\mathbf{Z}}$. Let $X = I(H(\mathbf{Z}') \leq x)$ and $X^{(d)} = I(H(\mathbf{Z}'^{(d)}) \leq x) \in [0, 1]$ for any $x \in \mathcal{R}$. By Hoeffding's Lemma, $\mathbb{E}_{\mathbf{Z}'^{(d)} | \mathbf{Z}} \exp(s(X^{(d)} - \mathbb{E}_{\mathbf{Z}'^{(d)} | \mathbf{Z}} X^{(d)})) \leq \exp(s^2/8)$ a.s. for any $s > 0$, where $\mathbb{E}_{\mathbf{Z}' | \mathbf{Z}}$ is the conditional expectation with respect to $\mathbf{Z}'^{(d)}$ given \mathbf{Z} . By Markov's inequality and the conditional independence

between $\mathbf{Z}'^{(1)}, \dots, \mathbf{Z}'^{(d)}$ given \mathbf{Z} , for any $t > 0$ and $s = 4t$,

$$\begin{aligned} & \Pr\left(\left|\tilde{F}_{H'}(\mathbf{x}) - \tilde{F}_H(\mathbf{x})\right| \geq t\right) \\ &= \Pr\left(\left|D^{-1} \sum_{d=1}^D X^{(d)} - \mathbb{E}_{\mathbf{Z}'^{(d)} | \mathbf{Z}} X^{(d)}\right| \geq t\right) \\ &\leq \exp(-sDt) \mathbb{E}_{\mathbf{Z}} \prod_{d=1}^D \mathbb{E}_{\mathbf{Z}'^{(d)} | \mathbf{Z}} (\exp(s(X^{(d)} - \mathbb{E}_{\mathbf{Z}'^{(d)} | \mathbf{Z}} X^{(d)}))) \\ &\leq \exp(-sDt) \exp(Ds^2/8) \leq \exp(-2Dt^2). \end{aligned}$$

For any $\delta \in (0, 1)$, by choosing $t = \sqrt{\frac{\log \frac{4}{\delta}}{2D}}$, we have $\left|\tilde{F}_{H'}(\mathbf{x}) - \tilde{F}_H(\mathbf{x})\right| \leq \sqrt{\frac{\log \frac{4}{\delta}}{2D}}$, with probability at least $1 - \delta$. On the other hand, $\left|\tilde{F}_H(\mathbf{x}) - F_H(\mathbf{x})\right| \leq \text{KS}(\tilde{F}_H, F_H) \leq \text{TV}(\tilde{\mathbf{Z}}, \mathbf{Z})$ with probability at least $1 - \frac{\delta}{2}$, where $\text{TV}(\tilde{\mathbf{Z}}, \mathbf{Z})$ is the total variation distance between the distributions of $\tilde{\mathbf{Z}}$ and \mathbf{Z} . Using the union bound to combine these foregoing results, we obtain that

$$\sup_{\mathbf{x}} \left|\tilde{F}_H(\mathbf{x}) - F_H(\mathbf{x})\right| \leq \sqrt{\frac{\log \frac{4}{\delta}}{2D}} + \text{TV}(\tilde{\mathbf{Z}}, \mathbf{Z}),$$

with probability at least $1 - \delta$. Note that $\text{TV}(\tilde{\mathbf{Z}}, \mathbf{Z}) = |\mathcal{S}| \cdot \text{TV}(\tilde{F}_{\mathbf{Z}}, F_{\mathbf{Z}})$. This completes the proof. \square

Proof of Theorem 2: In the setting of Theorem 1, note that $H(\mathbf{Z}) = T(\hat{\boldsymbol{\theta}}, \boldsymbol{\theta})$. By Theorem 3 of [41], the conditional distribution of $H' = H(\mathbf{Z}') = T(\hat{\boldsymbol{\theta}}^{(d)}, \hat{\boldsymbol{\theta}})$ given \mathbf{Z} remains the same as the distribution of $T(\boldsymbol{\theta}, \hat{\boldsymbol{\theta}})$ for any \mathbf{Z} , that is, for any event $\mathbf{x} \in \mathcal{R}^d$,

$$\begin{aligned} F_{H | \mathbf{Z}}(\mathbf{x}) &= \Pr(T(\hat{\boldsymbol{\theta}}^{(d)}, \hat{\boldsymbol{\theta}}) \leq \mathbf{x} | \mathbf{Z}) \\ &= \Pr(T(\hat{\boldsymbol{\theta}}, \boldsymbol{\theta}) \leq \mathbf{x}) = F_H(\mathbf{x}); d = 1, \dots, D, \end{aligned}$$

implying that $\text{Err}_H = 0$. This completes the proof. \square

REFERENCES

- [1] M. Berblinger and C. Schlier. Monte carlo integration with quasi-random numbers: some experience. *Computer physics communications*, 66(2-3):157–166, 1991.
- [2] X. Bi and X. Shen. Distribution-invariant differential privacy. *Journal of Econometrics*, DOI: //doi.org/10.1016/j.jeconom.2022.05.004, 2022.
- [3] A. Brock, J. Donahue, and K. Simonyan. Large scale gan training for high fidelity natural image synthesis. *arXiv preprint arXiv:1809.11096*, 2018.
- [4] V. Chernozhukov, D. Chetverikov, M. Demirer, E. Duflo, C. Hansen, W. Newey, and J. Robins. Double/debiased machine learning for treatment and structural parameters, 2018.
- [5] B. Dai, X. Shen, and W. Pan. Significance tests of feature relevance for a black-box learner. *IEEE Transactions on Neural Networks and Learning Systems*, //doi.org/10.1109/TNNLS.2022.3185742, 2022.
- [6] N. Deb, P. Ghosal, and B. Sen. Rates of estimation of optimal transport maps using plug-in estimators via barycentric projections. *Advances in Neural Information Processing Systems*, 34, 2021.
- [7] N. Deb and B. Sen. Multivariate rank-based distribution-free nonparametric testing using measure transportation. *Journal of the American Statistical Association*, 118(541):192–207, 2023.
- [8] B. Devezir, D. J. Navarro, J. Vandekerckhove, and E. Ozge Buzbas. The case for formal methodology in scientific reform. *Royal Society open science*, 8(3):200805, 2021.
- [9] J. Devlin, M.-W. Chang, K. Lee, and K. Toutanova. Bert: Pre-training of deep bidirectional transformers for language understanding. *arXiv preprint arXiv:1810.04805*, 2018.
- [10] P. Dhariwal and A. Nichol. Diffusion models beat gans on image synthesis. *Advances in Neural Information Processing Systems*, 34:8780–8794, 2021.

¹⁰A multivariate version of the fact that order statistics and rank statistics are independent.

- [11] L. Dinh, D. Krueger, and Y. Bengio. Nice: Non-linear independent components estimation. *arXiv preprint arXiv:1410.8516*, 2014.
- [12] L. Dinh, J. Sohl-Dickstein, and S. Bengio. Density estimation using real nvp. *arXiv preprint arXiv:1605.08803*, 2016.
- [13] B. Efron. Bootstrap methods: another look at the jackknife. In *Breakthroughs in statistics*, pages 569–593. Springer, 1992.
- [14] J. J. Faraway. Data splitting strategies for reducing the effect of model selection on inference. *Comput Sci Stat*, 30:332–41, 1998.
- [15] M. Germain, K. Gregor, I. Murray, and H. Larochelle. Made: Masked autoencoder for distribution estimation. In *International conference on machine learning*, pages 881–889. PMLR, 2015.
- [16] P. Ghosal and B. Sen. Multivariate ranks and quantiles using optimal transport: Consistency, rates and nonparametric testing. *The Annals of Statistics*, 50(2):1012–1037, 2022.
- [17] E. Gibney. Is ai fuelling a reproducibility crisis in science. *Nature*, 608:250–251, 2022.
- [18] M. Heusel, H. Ramsauer, T. Unterthiner, B. Nessler, and S. Hochreiter. Gans trained by a two time-scale update rule converge to a local nash equilibrium. *Advances in neural information processing systems*, 30, 2017.
- [19] J. Ho, A. Jain, and P. Abbeel. Denoising diffusion probabilistic models. *Advances in Neural Information Processing Systems*, 33:6840–6851, 2020.
- [20] J. Ho, C. Saharia, W. Chan, D. J. Fleet, M. Norouzi, and T. Salimans. Cascaded diffusion models for high fidelity image generation. *J. Mach. Learn. Res.*, 23:47–1, 2022.
- [21] M. Hollander, D. Wolfe, and E. Chicken. *Nonparametric Statistical Methods*. Wiley, New York, 3rd edition, 2013.
- [22] M. Hu and B. Liu. Mining and summarizing customer reviews. In *Proceedings of the tenth ACM SIGKDD international conference on Knowledge discovery and data mining*, pages 168–177, 2004.
- [23] R. Jonker and A. Volgenant. A shortest augmenting path algorithm for dense and sparse linear assignment problems. *Computing*, 38(4):325–340, 1987.
- [24] D. P. Kingma and P. Dhariwal. Glow: Generative flow with invertible 1x1 convolutions. *Advances in neural information processing systems*, 31, 2018.
- [25] D. P. Kingma and M. Welling. Auto-encoding variational bayes. *arXiv preprint arXiv:1312.6114*, 2013.
- [26] F. Koehler, V. Mehta, and A. Risteski. Representational aspects of depth and conditioning in normalizing flows. In *International Conference on Machine Learning*, pages 5628–5636. PMLR, 2021.
- [27] J. Komlós, P. Major, and G. Tusnády. An approximation of partial sums of independent rv’s, and the sample df. i. *Zeitschrift für Wahrscheinlichkeitstheorie und verwandte Gebiete*, 32:111–131, 1975.
- [28] A. Krizhevsky and G. Hinton. Learning multiple layers of features from tiny images. In *Proceedings of the 2009 conference on computer vision and pattern recognition*, pages 1378–1385. IEEE, 2009.
- [29] J. Lei, M. G’Sell, A. Rinaldo, R. J. Tibshirani, and L. Wasserman. Distribution-free predictive inference for regression. *Journal of the American Statistical Association*, 113(523):1094–1111, 2018.
- [30] A. Maas, R. E. Daly, P. T. Pham, D. Huang, A. Y. Ng, and C. Potts. Learning word vectors for sentiment analysis. In *Proceedings of the 49th annual meeting of the association for computational linguistics: Human language technologies*, pages 142–150, 2011.
- [31] R. J. McCann. Existence and uniqueness of monotone measure-preserving maps. *Duke Mathematical Journal*, 80(2):309–323, 1995.
- [32] T. Mikolov, K. Chen, G. Corrado, and J. Dean. Efficient estimation of word representations in vector space. In *Proceedings of the Workshop at ICLR*, 2013.
- [33] K. Oko, S. Akiyama, and T. Suzuki. Diffusion models are minimax optimal distribution estimators. *arXiv preprint arXiv:2303.01861*, 2023.
- [34] G. Papamakarios, E. T. Nalisnick, D. J. Rezende, S. Mohamed, and B. Lakshminarayanan. Normalizing flows for probabilistic modeling and inference. *J. Mach. Learn. Res.*, 22(57):1–64, 2021.
- [35] A. Radford, L. Metz, and S. Chintala. Unsupervised representation learning with deep convolutional generative adversarial networks. *arXiv preprint arXiv:1511.06434*, 2015.
- [36] A. Razavi, A. Van den Oord, and O. Vinyals. Generating diverse high-fidelity images with vq-vae-2. *Advances in neural information processing systems*, 32, 2019.
- [37] R. T. Rockafellar. *Convex analysis*, volume 11. Princeton university press, 1997.
- [38] R. Rombach, A. Blattmann, D. Lorenz, P. Esser, and B. Ommer. High-resolution image synthesis with latent diffusion models. In *Proceedings of the IEEE/CVF Conference on Computer Vision and Pattern Recognition*, pages 10684–10695, 2022.
- [39] O. Ronneberger, P. Fischer, and T. Brox. U-net: Convolutional networks for biomedical image segmentation. In *Medical Image Computing and Computer-Assisted Intervention–MICCAI 2015: 18th International Conference, Munich, Germany, October 5–9, 2015, Proceedings, Part III 18*, pages 234–241. Springer, 2015.
- [40] V. Sanh, L. Debut, J. Chaumond, and T. Wolf. Distilbert, a distilled version of bert: smaller, faster, cheaper and lighter. *arXiv preprint arXiv:1910.01108*, 2019.
- [41] X. Shen, X. Bi, and R. Shen. Data flush. *Harvard Data Science Review*, DOI: 10.1162/99608f92.681fe3bd, 2022.
- [42] X. Shen, W. Pan, Y. Zhu, and H. Zhou. On constrained and regularized high-dimensional regression. *Annals of the Institute of Statistical Mathematics*, 65(5):807–832, 2013.
- [43] L. N. Smith and N. Topin. Super-convergence: Very fast training of neural networks using large learning rates. In *Artificial intelligence and machine learning for multi-domain operations applications*, volume 11006, pages 369–386. SPIE, 2019.
- [44] J. Sohl-Dickstein, E. Weiss, N. Maheswaranathan, and S. Ganguli. Deep unsupervised learning using nonequilibrium thermodynamics. In *International Conference on Machine Learning*, pages 2256–2265. PMLR, 2015.
- [45] J. Song, C. Meng, and S. Ermon. Denoising diffusion implicit models. *arXiv:2010.02502*, October 2020.
- [46] C. Szegedy, S. Ioffe, V. Vanhoucke, and A. A. Alemi. Inception-v4, inception-resnet and the impact of residual connections on learning. In *Thirty-first AAAI conference on artificial intelligence*, 2017.
- [47] C. Szegedy, V. Vanhoucke, S. Ioffe, J. Shlens, and Z. Wojna. Rethinking the inception architecture for computer vision. In *Proceedings of the IEEE conference on computer vision and pattern recognition*, pages 2818–2826, 2016.
- [48] C. Villani. *Topics in optimal transportation*, volume 58. American Mathematical Soc., 2021.
- [49] L. Wasserman, A. Ramdas, and S. Balakrishnan. Universal inference. *Proceedings of the National Academy of Sciences*, 117(29):16880–16890, 2020.
- [50] L. Wasserman and K. Roeder. High dimensional variable selection. *Annals of statistics*, 37(5A):2178, 2009.
- [51] C.-H. Zhang and S. S. Zhang. Confidence intervals for low dimensional parameters in high dimensional linear models. *Journal of the Royal Statistical Society: Series B (Statistical Methodology)*, 76(1):217–242, 2014.
- [52] Z. Ziegler and A. Rush. Latent normalizing flows for discrete sequences. In *International Conference on Machine Learning*, pages 7673–7682. PMLR, 2019.

Supplementary Materials for Perturbation-Assisted Sample Synthesis: A Novel Approach for Uncertainty Quantification.

Yifei Liu, Rex Shen, Xiaotong Shen^{*}

I. LEARNING THEORY FOR NORMALIZING FLOWS

This section will leverage the maximum likelihood theory to derive novel results for normalizing flows. Initially, we present Lemma 1, which is a variant of Theorem 1 of [1] that is a penalized version of Theorem 1 of [4].

Let $\mathcal{F}_j = \{G \in \mathcal{F} : P(G) \leq j\}$. Define the metric entropy of \mathcal{F}_k under the Hellinger-distance $h(\cdot, \cdot)$. The approximation error for p_Z is $\gamma_{n_h} = \rho_\alpha^{1/2}(p_Z, \tilde{p}_Z) = \left(\mathbb{E} g_\alpha\left(\frac{p_Z}{\tilde{p}_Z}\right) \right)^{1/2}$, where $g_\alpha(x) = \alpha^{-1}(x^\alpha - 1)$ for $\alpha \in (0, 1)$, which is slightly stronger metric than the Kullback-Leibler divergence; c.f., Section 4 of [4].

Lemma 1 establishes the estimation error for the distribution under the total variation norm $\text{TV}(\tilde{F}_Z, F_Z)$ given fact that the total variation distance is upper bounded by the corresponding Hellinger-distance in that $\text{TV}(\tilde{F}_Z, F_Z) \leq h(\tilde{F}_Z, F_Z)$.

Lemma 1. (Estimation error of $F_Z = F_V \circ \tilde{G}^{-1}$ by PASS in (2)) Assume that $\tilde{Z} = (\tilde{Z}_i)_{i=1}^{n_h}$ is random sample following F_Z and \tilde{G} is the regularized MLE obtained from (2). Suppose there exist some positive constants C_1, C_2 , such that, for any $\epsilon_n > 0$, and $\lambda \geq 0$,

$$\sup_{j \geq 1} \int_{2^{-8} L_j}^{2^{1/2} L_j^{1/2}} H^{1/2}(u/C_2, \mathcal{F}_j) du / L_j \leq C_3 n_h^{1/2}, \quad (1)$$

where $L_j = C_1 \epsilon_n^2 + \lambda(j-1)$. Then $F_Z = F_V(\tilde{G}^{-1})$ satisfies:

$$P(h(F_Z, F_Z) \geq \eta_n) \leq 8 \exp(-C_4 n_h \eta_n^2),$$

with $\eta_{n_h} = \max(\epsilon_{n_h}, \gamma_{n_h})$ provided that λ is tuned: $\lambda \max(P(G^*), P(G), 1) \leq C_5 \eta_{n_h}^2$, $G^* \in \mathcal{F}$ is an approximating point of G , and $C_4 > 0$ is a constant. Hence, $h(\tilde{F}_Z, F_Z) = O_p(\eta_{n_h})$ as $n \rightarrow \infty$ under p_Z .

Now consider RealNVP flow [2], a normalizing flow with K affine-coupling layers with the reverse order permutation we used in Section V-B. Let $z_k = [z_k^{(1)}, z_k^{(2)}]$ be the output at k -th layer from its input $z_{k-1} = [z_{k-1}^{(1)}, z_{k-1}^{(2)}]$, and $[t_k, s_k] = f_{\theta_k}(z_{k-1}^{(1)})$ is a fully connected neural network parametrized by weights θ_k ; $k = 1, \dots$. Then, the coupling flow yields an output $T_\theta(z_0) = T_{\theta_K} \circ \dots \circ T_{\theta_1}$ from an input $z_0 = [z_0^{(1)}, z_0^{(2)}]$ (can be thought of as V_i 's, the latent representation in (1))

through function composition: $z_k = T_{\theta_K}(z_{k-1})$, defined recursively, via

$$z_k = \left[z_{k-1}^{(1)}, z_{k-1}^{(2)} \odot \exp(s_k) + t_k \right] P; k = 1, \dots, K, \quad (2)$$

where P is a $2d \times 2d$ permutation matrix whose entries are either 0 or 1 with the rows or columns arranged in the reverse order of the identity matrix, and \odot denotes the componentwise product. Note that each f_{θ_k} approximates a scale function s_k and a translation function t_k for $z_{k-1}^{(2)}$, while T_{θ_k} approximates a smooth and invertible function. Assume that d is independent of the sample size n_h . Let $\theta \equiv (\theta_1, \dots, \theta_K) \in \Theta \equiv \Theta_1 \times \dots \times \Theta_K$ represent the parameter of the normalizing flow. Denote \mathcal{T}_Θ as the class of K -layer affine coupling flow defined above parametrized by Θ . Using the framework of (2), we obtain that

$$\tilde{G} = \arg \max_{G_\theta \in \mathcal{T}_\Theta} n_h^{-1} \sum_{i=1}^{n_h} \log \left(p_V(G_\theta^{-1}(\tilde{Z}_i)) \cdot |\det J_{G_\theta}(G_\theta^{-1}(\tilde{Z}_i))|^{-1} \right) + \lambda P(G_\theta) \quad (3)$$

based on a holdout sample $(\tilde{Z}_i)_{i=1}^{n_h}$ from F_Z , the base density p_V , and the penalty function $P(G_\theta) = \|\theta\|_2^2$.

The following conditions are assumed:

Assumption 1 (Transport Approximation). The transport $G = T_\theta$ can be approximated by a normalizing flow with an approximation error $\gamma_{n_h} = \rho_\alpha^{1/2}(p_Z, \tilde{p}_Z)$ defined by the distance between the true density p_Z of Z and the best approximating density \tilde{p}_Z induced by the flow, for some $0 < \alpha < 1$.

Assumption 2 (Neural Networks). The fully connected neural networks remain the same structure for each layer of the flow, with a parameter space

$$\Theta_k = \{\theta_k : \max(\|\mathbf{W}_{k,l}\|_\infty, \|\mathbf{b}_{k,l}\|_\infty) \leq 1, \|\theta_k\|_0 \leq s_k\},$$

where $\theta_k = (\mathbf{W}_{k,l}, \mathbf{b}_{k,l})_{1 \leq l \leq h}$ are the network weight matrix and bias vector at flow layer k and neural network layer l , $\|\theta_k\|_0 = \sum_{l=0}^L (\|\mathbf{W}_{k,l}\|_0 + \|\mathbf{b}_{k,l}\|_0)$ is the L_0 -norm and $\|\cdot\|_\infty$ denotes the L_∞ -norm. For this network, the first layer consists of d nodes and equal width for middle and the layer consists of $2d$ layers. Total number of nonzero network parameters in the K -layer affine coupling flow is $s = \sum_{k=1}^K s_k$.

Assumption 3 (Base Density). The density of V $p_V(v)$ satisfies the Lipschitz condition with a Lipschitz constant L_p with respect to ℓ_2 norm. and B_p is the sup-norm of $p_V(v)$.

Lemma 2. Under Assumptions F1-F3, for any $\theta, \theta' \in \Theta$,

Yifei Liu is with School of Statistics, University of Minnesota, MN, 55455 USA (email: liu00980@umn.edu).

Rex Shen is with Department of Statistics, Stanford University, CA, 94305 USA (email: rshen0@stanford.edu).

Xiaotong Shen is with School of Statistics, University of Minnesota, MN, 55455 USA (email: xshen@umn.edu).

$\|p_{\theta} - p_{\theta'}\| \leq \sum_{k=1}^K A_k \|f_{\theta_k} - f_{\theta'_k}\|$, where

$$A_k = \exp(B_f dK) (L_p \left(C(B_f) \sqrt{d} \right)^k \prod_{m=1}^{k-1} (\tau_m \vee 1) + B_p C(B_f) d\tau_k),$$

where B_f is the ℓ_{∞} bound on both input vectors and output vectors of T_{θ_k} and f_{θ_k} for all $k = 1, \dots, K$; $C(B_f)$ is a universal constant depending on B_f only; τ_k is the Lipschitz constant of f_{θ_k} with respect to ℓ_2 norm in both input and output space.

Proof of Lemma 2: Let $T = T_K \circ \dots \circ T_1$ where $T_k \equiv T_{\theta_k}$; $k = 1, \dots, K$. Denote $\mathbf{z}_k = [\mathbf{z}_k^{(1)}, \mathbf{z}_k^{(2)}]$ as the corresponding output of k -th flow layer, and let $\mathbf{v} = T^{-1}(\mathbf{z})$ be the input of the flow, and \mathbf{z} is the final output; Let $[\mathbf{s}_k, \mathbf{t}_k] = f_{\theta_k}(\mathbf{z}_{k-1}^{(1)})$ be the scaling and translation parameters of k -th flow layer defined by a neural network f_{θ_k} ; Define $G_k = T_k \circ \dots \circ T_1$; $k = 1, \dots, K$. Define $T', T'_k, \mathbf{z}'_k, \mathbf{v}', [\mathbf{s}'_k, \mathbf{t}'_k]$ and G'_k similarly, but with another set of parameters $\theta' \in \Theta$. Let $p(\mathbf{v}) \equiv p_{\mathbf{V}}(\mathbf{v})$ be the base density and $p_{\theta}(\mathbf{z})$ be the parametrized density of the output of \mathbf{z} . For this proof, we will use $C(B_f)$ to indicate a function that only depends on constant B_f , which is not necessarily the same every time it appears, but remains a universal constant of B_f in any case.

We begin with the following decomposition,

$$\begin{aligned} & |p_{\theta}(\mathbf{z}) - p_{\theta'}(\mathbf{z})| \\ &= |p(\mathbf{v}) \cdot |\det J_T(\mathbf{v})|^{-1} - p(\mathbf{v}') \cdot |\det J_{T'}(\mathbf{v}')|^{-1}| \\ &\leq |p(\mathbf{v}) - p(\mathbf{v}')| \cdot |\det J_T(\mathbf{v})|^{-1} \\ &\quad + p(\mathbf{v}') \cdot \left| |\det J_T(\mathbf{v})|^{-1} - |\det J_{T'}(\mathbf{v}')|^{-1} \right| \\ &\leq L_p \|\mathbf{v} - \mathbf{v}'\|_2 \cdot |\det J_T(\mathbf{v})|^{-1} \\ &\quad + B_p \cdot \left| |\det J_T(\mathbf{v})|^{-1} - |\det J_{T'}(\mathbf{v}')|^{-1} \right| \\ &\leq L_p \exp(KB_f d) \|\mathbf{v} - \mathbf{v}'\|_2 \\ &\quad + B_p \cdot \left| |\det J_T(\mathbf{v})|^{-1} - |\det J_{T'}(\mathbf{v}')|^{-1} \right|. \end{aligned}$$

Next, we bound $A = \|\mathbf{v} - \mathbf{v}'\|_2$ and $B = \left| |\det J_T(\mathbf{v})|^{-1} - |\det J_{T'}(\mathbf{v}')|^{-1} \right|$ separately.

For A , note that

$$\begin{aligned} A &= \|\mathbf{v} - \mathbf{v}'\|_2 = \|T_1^{-1}(\mathbf{z}_1) - (T'_1)^{-1}(\mathbf{z}'_1)\|_2 \\ &\leq \|T_1^{-1}(\mathbf{z}_1) - T_1^{-1}(\mathbf{z}'_1)\|_2 + \|T_1^{-1}(\mathbf{z}'_1) - (T'_1)^{-1}(\mathbf{z}'_1)\|_2 \\ &\leq C(B_f) \sqrt{d} (\tau_1 \vee 1) \cdot \|\mathbf{z}_1 - \mathbf{z}'_1\|_2 \\ &\quad + C(B_f) \sqrt{d} \cdot \|f_{\theta_1}(\mathbf{z}'_1) - f_{\theta'_1}(\mathbf{z}'_1)\|_2, \end{aligned}$$

where we use the Lipschitz property of T_1^{-1} for the first term, and the difference between T_1^{-1} and $(T'_1)^{-1}$ for the second term. See Lemmas 3 and 4 for the derivation of these two bounds. Then a deduction can be done to bound $\|\mathbf{z}_1 - \mathbf{z}'_1\|_2$ in a similar way as above, which gives the final bound as follows,

$$\begin{aligned} A &\leq \sum_{k=1}^K \left(C(B_f) \sqrt{d} \right)^k \prod_{m=1}^{k-1} (\tau_m \vee 1) \|f_{\theta_k}(\mathbf{z}'_k) - f_{\theta'_k}(\mathbf{z}'_k)\|_2 \\ &\leq \sum_{k=1}^K \left(C(B_f) \sqrt{d} \right)^k \prod_{m=1}^{k-1} (\tau_m \vee 1) \|f_{\theta_k} - f_{\theta'_k}\|_{\infty}. \end{aligned}$$

For B , note that

$$\begin{aligned} |\det J_T(\mathbf{v})|^{-1} &= \exp(-\mathbf{1}^{\top} \mathbf{s}_K) \cdot |\det J_{G_{K-1}}(\mathbf{v})|^{-1} \\ &= \dots = \exp(-\mathbf{1}^{\top} (\mathbf{s}_K + \dots + \mathbf{s}_1)). \end{aligned}$$

Then,

$$\begin{aligned} B &= \left| |\det J_T(\mathbf{v})|^{-1} - |\det J_{T'}(\mathbf{v}')|^{-1} \right| \\ &\leq \exp(-\mathbf{1}^{\top} \mathbf{s}_K) \cdot \left| |\det J_{G_{K-1}}(\mathbf{v})|^{-1} - |\det J_{G'_{K-1}}(\mathbf{v}')|^{-1} \right| \\ &\quad + \left| \det J_{G'_{K-1}}(\mathbf{v}') \right|^{-1} \cdot \left| \exp(-\mathbf{1}^{\top} \mathbf{s}_K) - \exp(-\mathbf{1}^{\top} \mathbf{s}'_K) \right| \\ &\leq \exp(dB_f) \cdot \left| |\det J_{G_{K-1}}(\mathbf{v})|^{-1} - |\det J_{G'_{K-1}}(\mathbf{v}')|^{-1} \right| \\ &\quad + \exp(d(K-1)B_f) \cdot \left| \exp(-\mathbf{1}^{\top} \mathbf{s}_K) - \exp(-\mathbf{1}^{\top} \mathbf{s}'_K) \right|. \end{aligned}$$

To bound the second term on RHS, we first notice that $\exp(-\mathbf{1}^{\top} \mathbf{s})$ is $\sqrt{d} \exp(dB_f)$ -Lipschitz with respect to $\|\cdot\|_2$, which gives us, for any $\mathbf{s}_K, \mathbf{s}'_K \in \mathcal{R}^d$,

$$\left| \exp(-\mathbf{1}^{\top} \mathbf{s}_K) - \exp(-\mathbf{1}^{\top} \mathbf{s}'_K) \right| \leq \sqrt{d} \exp(dB_f) \cdot \|\mathbf{s}_K - \mathbf{s}'_K\|_2.$$

It remains to bound $\|\mathbf{s}_K - \mathbf{s}'_K\|_2$, which we proceed as follows, with a general $k = 1, \dots, K$ instead:

$$\begin{aligned} & \|\mathbf{s}_k - \mathbf{s}'_k\|_2 \\ &= \|f_{\theta_k}(\mathbf{z}_{k-1}^{(1)}) - f_{\theta'_k}(\mathbf{z}'_{k-1})\|_2 \\ &\leq \|f_{\theta_k}(\mathbf{z}_{k-1}^{(1)}) - f_{\theta_k}(\mathbf{z}'_{k-1})\|_2 + \|f_{\theta_k}(\mathbf{z}'_{k-1}) - f_{\theta'_k}(\mathbf{z}'_{k-1})\|_2 \\ &\leq \tau_k \|\mathbf{z}_{k-1} - \mathbf{z}'_{k-1}\|_2 + \|f_{\theta_k}(\mathbf{z}'_{k-1}) - f_{\theta'_k}(\mathbf{z}'_{k-1})\|_2 \\ &\leq \tau_k C(B_f) \sqrt{d} \|f_{\theta_k}(\mathbf{z}_k) - f_{\theta'_k}(\mathbf{z}_k)\|_2 + \|f_{\theta_k}(\mathbf{z}'_{k-1}) - f_{\theta'_k}(\mathbf{z}'_{k-1})\|_2, \end{aligned}$$

where we use Lemma 4 again for the last inequality. After cleaning and arranging some terms, we obtain the bound

$$\begin{aligned} B &\leq \exp(dB_f) \cdot \left| |\det J_{G_{K-1}}(\mathbf{v})|^{-1} - |\det J_{G'_{K-1}}(\mathbf{v}')|^{-1} \right| \\ &\quad + d \exp(dKB_f) \tau_K C(B_f) \cdot \|f_{\theta_K} - f_{\theta'_K}\|_{\infty}, \end{aligned}$$

which, by deduction on $\left| |\det J_{G_{K-1}}(\mathbf{v})|^{-1} - |\det J_{G'_{K-1}}(\mathbf{v}')|^{-1} \right|$, gives the following bound

$$B \leq C(B_f) d \exp(KdB_f) \cdot \sum_{k=1}^K \tau_k \|f_{\theta_k} - f_{\theta'_k}\|_{\infty}.$$

Finally, we combine bounds on A and B to obtain the desired bound in Lemma 2. \square

Next we present Lemma 3 and 4 used in the proof of Lemma 2, along with their proofs.

Lemma 3. Consider one affine coupling layer $f : [\mathbf{x}^{(1)}, \mathbf{x}^{(2)}] \in \mathcal{R}^{2d} \mapsto [\mathbf{x}^{(1)}, \mathbf{x}^{(2)} \odot \exp(s) + t]P \in \mathcal{R}^{2d}$ where $[s, t] = g(\mathbf{x}^{(1)})$ is a neural network mapping from \mathcal{R}^d to \mathcal{R}^{2d} , with Lipschitz constant $\tau > 0$ w.r.t. $\|\cdot\|_2$. Let $B_f > 0$ be the ℓ_{∞} bound on both input and output vectors of f and g . Then for any $\mathbf{z}, \mathbf{y} \in \mathcal{R}^{2d}$, we have $\|f^{-1}(\mathbf{z}) - f^{-1}(\mathbf{y})\|_2 \leq C(B_f) \sqrt{d} (\tau \vee 1) \cdot \|\mathbf{z} - \mathbf{y}\|_2$.

Proof of Lemma 3: By definition of f ,

$$\begin{aligned} \|f^{-1}(\mathbf{z}) - f^{-1}(\mathbf{y})\|_2 &\leq \|\mathbf{z}^{(1)} - \mathbf{y}^{(1)}\|_2 \\ &\quad + \|\mathbf{z}^{(2)} \odot \exp(-s(\mathbf{z}^{(1)})) - \mathbf{y}^{(2)} \odot \exp(-s(\mathbf{y}^{(1)}))\|_2 \\ &\quad + \|t(\mathbf{z}^{(1)}) \odot \exp(-s(\mathbf{z}^{(1)})) - t(\mathbf{y}^{(1)}) \odot \exp(-s(\mathbf{y}^{(1)}))\|_2. \end{aligned}$$

The second term on RHS can be bounded:

$$\begin{aligned}
& \| \mathbf{z}^{(2)} \odot \exp(-s(\mathbf{z}^{(1)})) - \mathbf{y}^{(2)} \odot \exp(-s(\mathbf{y}^{(1)})) \|_2 \\
& \leq \| \mathbf{z}^{(2)} \|_2 \cdot \| \exp(-s(\mathbf{z}^{(1)})) - \exp(-s(\mathbf{y}^{(1)})) \|_2 \\
& \quad + \| \mathbf{z}^{(2)} - \mathbf{y}^{(2)} \|_2 \cdot \| \exp(-s(\mathbf{y}^{(1)})) \|_2 \\
& \leq \sqrt{d} B_f \exp(B_f) \cdot \| s(\mathbf{z}^{(1)}) - s(\mathbf{y}^{(1)}) \|_2 \\
& \quad + \sqrt{d} \exp(B_f) \cdot \| \mathbf{z}^{(2)} - \mathbf{y}^{(2)} \|_2 \\
& \leq \sqrt{d} B_f \exp(B_f) \tau \cdot \| \mathbf{z}^{(1)} - \mathbf{y}^{(1)} \|_2 \\
& \quad + \sqrt{d} \exp(B_f) \cdot \| \mathbf{z}^{(2)} - \mathbf{y}^{(2)} \|_2.
\end{aligned}$$

The third term on RHS can be bounded:

$$\begin{aligned}
& \| t(\mathbf{z}^{(1)}) \odot \exp(-s(\mathbf{z}^{(1)})) - t(\mathbf{y}^{(1)}) \odot \exp(-s(\mathbf{y}^{(1)})) \|_2 \\
& \leq \| t(\mathbf{z}^{(1)}) \|_2 \cdot \| \exp(-s(\mathbf{z}^{(1)})) - \exp(-s(\mathbf{y}^{(1)})) \|_2 \\
& \quad + \| \exp(-s(\mathbf{y}^{(1)})) \|_2 \cdot \| t(\mathbf{z}^{(1)}) - t(\mathbf{y}^{(1)}) \|_2 \\
& \leq \sqrt{d} B_f \exp(B_f) \cdot \| s(\mathbf{z}^{(1)}) - s(\mathbf{y}^{(1)}) \|_2 \\
& \quad + \sqrt{d} \exp(B_f) \cdot \| t(\mathbf{z}^{(1)}) - t(\mathbf{y}^{(1)}) \|_2 \\
& \leq \left(\sqrt{d} B_f \exp(B_f) + \sqrt{d} \exp(B_f) \right) \cdot \| g(\mathbf{z}^{(1)}) - g(\mathbf{y}^{(1)}) \|_2 \\
& \leq \left(\sqrt{d} B_f \exp(B_f) + \sqrt{d} \exp(B_f) \right) \tau \cdot \| \mathbf{z}^{(1)} - \mathbf{y}^{(1)} \|_2.
\end{aligned}$$

Combining all terms together, we have the desired result in Lemma 3, implying that the Lipschitz constant of f^{-1} is $C(B_f)\sqrt{d}(\tau \vee 1)$. \square

Lemma 4. Consider two affine coupling layers f_1 and f_2 defined in the same way as in Lemma 3, using neural networks g_1 and g_2 to generate scaling and translation parameters $[s_1, t_1]$ and $[s_2, t_2]$, respectively. Then for any $\mathbf{y} \in \mathcal{R}^{2d}$, we have $\|f_1^{-1}(\mathbf{y}) - f_2^{-1}(\mathbf{y})\|_2 \leq C(B_f)\sqrt{d} \cdot \|g_1(\mathbf{y}^{(1)}) - g_2(\mathbf{y}^{(1)})\|_2$.

Proof of Lemma 4: Using the definition of f_1 and f_2 , we begin with the following decomposition,

$$\begin{aligned}
& \|f_1^{-1}(\mathbf{y}) - f_2^{-1}(\mathbf{y})\|_2 \\
& \leq \| \mathbf{y}^{(2)} \odot \left(\exp(-s_1(\mathbf{y}^{(1)})) - \exp(-s_2(\mathbf{y}^{(1)})) \right) \|_2 \\
& \quad + \| t_1(\mathbf{y}^{(1)}) \odot \exp(-s_1(\mathbf{y}^{(1)})) - t_2(\mathbf{y}^{(1)}) \odot \exp(-s_2(\mathbf{y}^{(1)})) \|_2.
\end{aligned}$$

Then, using a similar argument in the proof of Lemma 3, the first term on RHS can be bounded by $\sqrt{d} B_f \exp(B_f) \cdot \|s_1(\mathbf{y}^{(1)}) - s_2(\mathbf{y}^{(1)})\|_2$, while the second term can be bounded by

$$\begin{aligned}
& \sqrt{d} B_f \exp(B_f) \cdot \|s_1(\mathbf{y}^{(1)}) - s_2(\mathbf{y}^{(1)})\|_2 \\
& \quad + \sqrt{d} \exp(B_f) \cdot \|t_1(\mathbf{y}^{(1)}) - t_2(\mathbf{y}^{(1)})\|_2,
\end{aligned}$$

which, combined together, give the desired bound. \square

In the literature, [3] demonstrates how normalizing flows can be used as a universal approximator to complex distributions. As suggested by [3], even shallow affine coupling networks can approximate a smooth and invertible transport in Wasserstein distance well, as in GLOW. Yet, the approximation error bounds have not been available for essentially any flows.

Proposition 1. (Validity of PAI inference for the test (6)) Under Assumptions 1-3, the maximum likelihood transport \hat{G} from (3) by RealNVP with the reverse permutation and a fully

connected neural network satisfies:

$$h(\tilde{F}_Z, F_Z) = O_p \left(\max \left(\left(\frac{s}{n_h} \log \frac{n_h}{s} \right)^{1/2}, \gamma_d \right) \right), \quad (4)$$

where γ_d is the approximation error and s the number of non-zero parameters in the neural network. In conclusion, by (3), the PAI test in (4) is valid for any inference sample $\mathbb{S} = (\mathbf{X}_i, Y_i)_{i=1}^{n_h}$ as the holdout size $n_h \rightarrow \infty$ and the MC size $D \rightarrow \infty$.

Proof of Proposition 1: To apply Lemma 1, we bound the metric entropy and compute the approximation error.

Approximation Error. By Assumption 3 and Lemma 2, $\gamma_{n_d} \leq C_5 \|p_{\theta^*} - p_{\theta^0}\|_\infty \leq C_5 \epsilon$ for some constant $C_5 > 0$, or approximation error $\gamma_d = \rho_{0+}^\alpha(p_Z, \tilde{p}_Z) = C_5 \sqrt{d} \epsilon$, where ρ_{0+}^α is the Kullback–Leibler divergence that is upper bounded by the corresponding Hellinger-distance when the densities are bounded away from zero and infinity.

Metric Entropy. Note that $\mathcal{F}_j = \{\theta \in \mathcal{F} : \lambda P(G) \leq j, \|\theta - \theta^0\|_2 < 2\epsilon\}$ is uniformly bounded. Let $\mathcal{S}_\infty(u, m)$ be a u -cover of \mathcal{F}_j in $\|\cdot\|_\infty$. Define $g_k^+ = g_k + u$ and $g_k^- = g_k - u$, where $g_k \in \mathcal{S}_\infty(u, m)$, $k = 1, \dots, m$. Then $\{g_1^\pm, \dots, g_m^\pm\}$ forms a u -bracket of \mathcal{F}_j . Hence, $H(u, \mathcal{F}_j) = \min_m \log m \leq H_\infty(u, \mathcal{F}_j)$, where $H_\infty(u, \cdot)$ denotes the entropy under the sup-norm. Then, by Lemma 2,

$$H_\infty(u, \mathcal{F}_j) \leq s \left(\log \left(\frac{\max(j, 1)}{u} \right) \right).$$

Thus, the entropy integral in (1) becomes

$$\begin{aligned}
& \int_{\epsilon^2/256}^{\sqrt{2}\epsilon} H_B^{1/2}(u/c_1, \mathcal{F}_j(A_j)) du \leq \int_{\epsilon^2/256}^{\sqrt{2}\epsilon} \sqrt{s} \sqrt{\log \left(\frac{\max(j, 1)}{u} \right)} du \\
& \leq C_5 \sqrt{s} (\log(1/\epsilon))^{1/2} \epsilon.
\end{aligned}$$

We solve the integral equation:

$$C_5 \sqrt{s} (\log(1/\epsilon))^{1/2} \epsilon \leq C_6 \epsilon^2 \sqrt{n_h},$$

$\epsilon \asymp \sqrt{\frac{s}{n_h} \log \frac{n_h}{s}}$. Hence, $\eta_{n_h} = \max(\epsilon, \gamma_d)$ by Lemma 1. This completes the proof. \square

REFERENCES

- [1] B. Dai, X. Shen, and W. Wong. Coupled generation. *Journal of the American Statistical Association*, 117(539):1243–1253, 2022.
- [2] L. Dinh, J. Sohl-Dickstein, and S. Bengio. Density estimation using real nvp. *arXiv preprint arXiv:1605.08803*, 2016.
- [3] F. Koehler, V. Mehta, and A. Risteski. Representational aspects of depth and conditioning in normalizing flows. In *International Conference on Machine Learning*, pages 5628–5636. PMLR, 2021.
- [4] W. H. Wong and X. Shen. Probability inequalities for likelihood ratios and convergence rates of sieve MLEs. *The Annals of Statistics*, 23(2):339–362, 1995.